Engineering of redox-triggered polymeric lipid hybrid nanocarriers for selective drug delivery to cancer cells

Lokesh, B. Siva; AJMEERA, Suresh; Choudhary, Rajat; Moharana, Sanjaya Kumar; Purohit, C. S. & Konkimalla, V. Badireenath (2024) Engineering of redox-triggered polymeric lipid hybrid nanocarriers for selective drug delivery to cancer cells. In: Journal of materials chemistry B, 13 (4), p. 1437-1458.

DOI: 10.1039/d4tb01236d
Handle: http://hdl.handle.net/1942/44936

Engineering of Redox-triggered Polymeric Lipid Hybrid Nanocarriers for Selective Drug Delivery to Cancer Cells

B. Siva Lokesh [a, c, #], Suresh Ajmeera [a, d, e, #], Rajat Choudhary [a, c], Sanjaya Kumar Moharana [b,c], C. S. Purohit [b, c], V Badireenath Konkimalla [a, c] *

[a] School of Biological Sciences, National Institute of Science Education and Research, HBNI, Jatni, Odisha 752050, India

[b] School of Chemical Sciences, National Institute of Science Education and Research, HBNI, Jatni, Odisha 752050, India

[c] Homi Bhabha National Institute, Training School Complex, Anushakti Nagar, Mumbai 400094, India

[d] Hasselt University, Institute for Materials Research (IMO), Nano-Biophysics and Soft Matter Interfaces (NSI), Wetenschapspark 1, 3590 Diepenbeek, Belgium

[e] IMEC, associated lab IMOMEC, Wetenschapspark 1, 3590 Diepenbeek, Belgium

[*] Corresponding Author

[#] Equal Contribution

[*] **Corresponding author:**

Dr. V Badireenath Konkimalla

School of Biological Sciences,

National Institute of Science Education & Research (NISER), PO- Bhimpur-Padanpur, Via-Jatni, District: - Khurda, Bhubaneswar, Orissa - 752 050, INDIA

E-mail: badireenath@niser.ac.in (V.B. Konkimalla)

Tel: +91-674-249 42 11

Abstract

Tunable redox-sensitive polymeric-lipid hybrid nanocarriers (RS-PLHNCs) were fabricated using homogenization and nanoprecipitation methods. These nanocarriers composed of novel redox-cholesterol with disulfide linkages synthesized by conjugating cholesterol with dithiodipropionic acid *via* esterification. Berberine (BBR) was loaded into these fabricated nanocarriers to investigate the selective uptake of BBR by cancer cells, release, and enhanced cytotoxicity. The optimized BBR nanocarriers (BBR NP-**17** and **18**) exhibited a spherical shape and uniform distribution, with a particle size of 124.7±1.2 nm, 185.2±1.6 nm, and a zeta potential of -5.9±2.5 mV; -20.3±1.1 mV respectively. These NCs released > 80% BBR in the simulated intracellular tumor microenvironment (TME), while only 30-45% was released under normal physiological conditions. The accelerated drug release in the TME was due to disulfide bond cleavage and ester bond hydrolysis in the presence of GSH and acidic pH, whereas in normal conditions, the NCs remained stable/undissociated. Cellular uptake studies confirmed enhanced BBR uptake in GSH-rich cancer cells (H1975) over normal cells (BEAS-2B and HEK293A). Following uptake, these optimized nanocarriers displayed significant selective cytotoxicity and apoptosis in cancer cells by notably downregulating anti-oxidant (NFE2L2, HO-1, NQO1, and TXRND1), anti-apoptotic (MCL-1) genes, while upregulating pro-apoptotic genes (PUMA and NOXA) more than free form of the drug. This resulted in increased oxidative stress, thereby inducing selective apoptosis in the GSH-rich lung cancer cells. These results suggest that the synthesized novel NCs might hold great potential in specifically delivering drugs to cancer cells (with reduced environment), while baring the normal cells, thus ensuring safe and efficient cancer therapy.

Keywords: Tumor microenvironment; polymeric lipid hybrid nanocarriers; Cholesterol-Dithiodipropionate; redox-responsive delivery; Berberine; biocompatibility.

Abbreviations

BBR- Berberine, CL- Cholesterol, %DL- % Drug loading, DPPC- 1,2-Dipalmitoyl-sn-glycero-3-phosphocholine, DTDPA- Dithiodipropionate, DTPA- 3,3[1] Dithiodipropionic acid, %EE- %Entrapment efficiency, PDI - polydispersity index, PEG- Polyethylene glycol, PNIPAM- P-(N-isopropyl acrylamide), MTT- (3-(4,5-Dimethylthiazol-2-yl)-2,5-Diphenyltetrazolium Bromide), and RS-PLHNCs- Redox-sensitive polymeric lipid hybrid nanocarriers.

1. Introduction

Nanoscale drug delivery systems (NDDS) have emerged as a pivotal advancement in circumventing various pitfalls of traditional drug-delivery systems. This technological advancement has proved as a valuable carrier of several drugs, nucleic acids, and proteins in combating several cancers by overcoming biological barriers. Lipid and polymer-based nanocarriers have been widely explored in the past decade. Commercial examples of these nanocarriers include DOXIL® (Doxorubicin loaded PEGylated liposome), DaunoXome® (Daunorubicin liposome), DepoCyt® (Cytarabine liposome), Abraxane (Paclitaxel albumin nanoparticle), and Oncaspar® (Polymer protein conjugate of L-asparaginase). These nanocarriers offer several advantages in drug delivery, including enhancements in solubility, permeability, and bioavailability, protection from enzymatic degradation and harsh gastrointestinal conditions, increased half-life, and mitigation of off-target effects induced by toxic drug molecules.[1] Despite their promising potential in treating several cancers, these systems suffer from drawbacks such as poor entrapment, drug loading, and premature drug release.[2] Therefore, combining these systems may confer positive attributes of both systems that aid in overcoming individual limitations.

Polymeric lipid hybrid nanocarriers (PLHNCs) of 100-200 nm size are an ideal strategy that facilitates the effective delivery of different drugs into cancer cells *via* enhanced permeability and retention effect (EPR). These systems consist of a polymer core surrounded by a lipid layer, which enables the effective loading of hydrophobic and hydrophilic drugs in the polymer core and lipid matrix.[3] These novel systems offer several advantages in drug delivery; however, premature leakage of drugs during circulation and unintended release of drugs in healthy cells often results in side effects posing a significant challenge. To address these challenges and enhance the precise release of drugs in tumor sites, various unique factors prevailing in the endogenous tumor microenvironment (TME), such as pH, glutathione, reactive oxygen species, etc, have been explored to deliver the drugs in response to specific stimulus.

TME-responsive nanocarriers have garnered considerable attention in cancer therapy over external stimuli-responsive nanocarriers (e.g., magnetic, light, and ultrasound) by eliminating the need for additional instruments for drug release at the target site, thus making them more cost-effective. The prevailing endogenous environment of tumor cells/tissues that differ from the normal cells aids in designing a specialized nanocarrier system to release the drugs selectively in response to TME, barring the healthy cells. The intrinsic tumor

endogenous stimuli such as the extra and intracellular pH (pH 6.4 to 4.5 due to lactic acidosis)[4], several overexpressing proteins/enzymes, reductases (overexpressed in a hypoxia environment)[5,6], and intracellular reductive environment (elevated levels of GSH, i.e., about 2-10 mM of GSH concentration in tumor cells and 2-20 μM in healthy cells)[7] are the potential targets that are being explored. Due to these distinct microenvironment characteristics, many researchers have designed intelligent nanoparticles to deliver the drugs in response to endogenous stimuli. For instance, the inclusion of pH-sensitive groups like schiff base[8,9], hydrazone bonds[10,11], imine bonds[12], and ester bonds[13] in nanoformulation releases the drug in response to tumor acidic pH. Additionally, presence of nitroimidazole (NI)[14] and azobenzene (Azo)[6] derivatives trigger the drug release in response to overexpressed biological reductases (e.g., nitro reductases) in the hypoxic tumors and incorporation of disulfide bonds in the nanoparticle system responds to increased GSH levels in the intracellular TME.[15,16]

Berberine (BBR), a natural isoquinoline phytochemical, is recognized for its diverse pharmacological activities, including anti-cancer, anti-inflammatory, antimicrobial, and antioxidant activities. Despite its promising therapeutic potential, BBR is categorized as a class IV drug due to its poor solubility, low bioavailability, and limited cellular permeability. Moreover, the short half-life of BBR is a major limitation which decreases the therapeutic efficacy of the drug. However, to fulfill therapeutic requirements, higher doses of BBR have been employed, which could lead to adverse effects such as anorexia, stomach upset, diarrhea, or constipation, potentially compromising its therapeutic advantages.[22–25]

Recently, several nanoparticular delivery systems have been developed to minimize the limitations and enhance the therapeutic efficacy of BBR in cancer (albumin nanoparticles[22], nano lipid carriers[24], and chitosan NPs[26]). However, the selective release of BBR from the nanosystem at the cancer cell target remained less explored. To address the selectivity problem and potentiate therapeutic effectiveness, we aim to synthesize nanomaterials responsive to internal stimuli such as pH and GSH using biocompatible lipids (cholesterol[17], DPPC[18], and stearic acid[19]) and polymers (PEG[20] and PNIPAM[21]) for the loading and delivery of BBR in GSH rich cancer cells.

Therefore, in this study, a novel cholesterol lipid containing a disulfide (-S-S-) bond as a stimuli-responsive material was synthesized. This bio-reducible lipid was incorporated into **r**edox-**s**ensitive **p**olymeric **l**ipid **h**ybrid **n**anocarriers (RS-PLHNCs) with BBR loaded into the

nanocarrier system. The objective was to investigate the superiority of the synthesized nanocarrier system over free form of BBR in enhancing cancer cell selectivity and killing efficiency in non-small cell lung cancer cells (NSCLC; H1975 cells) *in vitro*, while also comparing its selectivity on normal lung and embryonic kidney cells (BEAS-2B and HEK293A cells). The efficacy of the nanoformulation is also dependent on its lipid composition, particle size, zeta potential, and the physicochemical characteristics of the loaded drug for its release and therapeutic activity. Therefore, different RS-PLHNCs of varying lipid composition were prepared and studied.

2. Experimental section

2.1. Materials

Berberine (BBR) and stearic acid were purchased from M.P. Biomedicals. Sodium azide (NaN_3), 4-toluenesulfonyl chloride (TsCl), 3,3[1]-dithiodipropionic acid (DTPA), triphenylphosphine (PPh3), 4-dimethylaminopyridine (DMAP), pluronic F-127 (PF-127) were procured from Sigma-Aldrich. Span-80, potassium hydroxide (KOH), absolute ethanol, dimethyl sulfoxide (DMSO), 3-(4,5-Dimethylthiazol-2-yl)-2,5-Diphenyltetrazolium Bromide (MTT), and L-Glutathione reduced (GSH) were purchased from Himedia. Dialysis membrane (10 KDa) was obtained from Invitrogen, poly-(N-isopropyl acrylamide) from TCI chemicals, polyethylene glycol (PEG) (M.wt. 2000 g mol^{-1}) from Alfa Aesar, cholesterol (CL) from Bio world, acetic anhydride from Pallav chemicals, toluene from SRL, and dipalmitoyl phosphatidylcholine (DPPC) from Avanti polar lipids.

All solvents used to synthesize modified lipids and polymers were purchased from Spectrochem. Dichloromethane (DCM), diethyl ether, dimethyl formamide (DMF, dry), methanol (MeOH), tetrahydrofuran (THF), n-hexane, pyridine (dry), ethyl acetate, and acetonitrile.

2.2. Synthesis of redox-sensitive disulfide cholesterol (Cholesterol-Dithiodipropionate)

Cholesterol-dithiodipropionate (CL-DTDPA) was synthesized following a reported method with slight modifications.[27] Briefly, 3,3[1]dithiodipropionic acid (1 g, 4.755 mmol) was dissolved in acetic anhydride (75 mL) and stirred for 3-4 h under N_2 atmosphere to obtain dithiodipropionic anhydride (DTDPA). To the above DTDPA solution, toluene (10-15 mL) was added and dried under reduced pressure using a rotary evaporator (Heidolph Rotary evaporator) three to four times. The obtained pure DTDPA residue was dissolved in dry

DCM (50 mL) and admixed with CL (1.838 g, 4.755 mmol) and DMAP (0.290 g, 2.377 mmol). Then, the reaction mixture was continuously agitated at room temperature in inert N_2 atmospheric conditions, and simultaneously, the progress of the reaction was monitored using TLC. The resulting product was extracted with a DCM / water system. The organic layer was collected, washed several times with water, dried with anhydrous Na_2SO_4, and evaporated using a rotary evaporator. The acquired product was finally purified using silica-gel column chromatography (stationary phase: silica gel (mesh size: 100-200); mobile phase: 10-30% ethyl acetate and hexane), the eluted mobile phase was evaporated, washed with acetonitrile, and dried under reduced pressure to obtain pure CL-DTDPA (CL-COO-SS-COOH).[28] The purified CL-DTDPA was further characterized for ^{1}H NMR and ^{13}C NMR to verify the structure. The obtained pure CL-DTDPA (redox-CL) was used for the fabrication of redox-sensitive PLHNCs.

The final yield was 80%. ^{1}H NMR ($CDCl_3$, ppm): δ 5.38 (1H, =CH-), 4.65 (1H, -CH-), 2.93(4H, -CH_2-SS-), 2.80 (2H, -CH_2-COOH), and 2.72 (2H, -CH_2-COO-) (Fig. 1A). ^{13}C NMR ($CDCl_3$, ppm): δ 177.94 (-COOH), and 171.02 (-COO-) (Fig. 1B). ESI-MS (m/z): $C_{33}H_{54}O_4S_2$ - 579.35 $[M + H]^+$ (Fig. S2A).

2.3. Synthesis of polyethylene glycol diamine (PEGDA)

2.3.1. Synthesis of Tosylated PEG

Tosylated PEG (TS-PEG) was synthesized by dissolving PEG-2000 (1.00 g, 0.5 mmol) in DCM (50 mL), followed by the addition of tosyl chloride (0.23 g, 1.25 mmol). Later, KOH powder was added slowly to the above reaction mixture in ice-cold conditions (0-8°C) and allowed to react overnight under agitation at room temperature. The obtained mixture was extracted with DCM / distilled water, and the organic layer was collected, washed, and vacuum-dried. The concentrated oily product was precipitated by adding excess diethyl ether, filtered, washed, and dried under vacuum to get a solid product of pure TS-PEG.[29] Thus, synthesized TS-PEG was further used to prepare PEG Diazide without further purification.

The final yield was 98%. ^{1}H NMR (d6-DMSO, ppm): 7.77 (=CH-), 7.48 (=CH-), 4.09 (-CH_2-O-), 3.31 - 3.66 (-CH_2-CH_2-O-), and 2.4 (-CH_2) (Fig. S1A). ^{13}C NMR (d6-DMSO, ppm): 145.41 (C), 132.8 (=CH-), 130.59 (=CH-), 128.03 (C), 70.3 (-CH_2-CH_2-O-), and 68.3 (-CH_2-O-) (Fig. S1B).

2.3.2. Synthesis of PEG Diazide

PEG Diazide (PEGD) was synthesized using a substitution mechanism. In brief, the obtained TS-PEG (0.5 g, 0.21 mmol) was dissolved in dry DMF (minimum solubility) and supplemented with sodium azide (0.03 g, 0.54 mmol). After gentle stirring, the reaction mixture temperature was raised slowly to 80^{o}C under an inert N_2 atmosphere, and the mixture was continued stirring for another 24 h. The resulting solution was evaporated and extracted with DCM, distilled water, and cold brine solution several times. The organic layer was separated and evaporated, and the obtained solid product was purified using silica column chromatography (stationary phase: silica gel (mesh size: 100-200), mobile phase: 2-5% MeOH and DCM). Finally, the eluted mobile phase was evaporated, washed with diethyl ether, and vacuum-dried to obtain PEGD.[29]

The final yield was 80%. ^{1}H NMR (d6-DMSO, ppm): δ 3.46 – 3.67 (-CH_2-CH_2-O), and 3.37 (-CH_2-N_3) (Fig. S1C). ^{13}C NMR (d6-DMSO, ppm): δ 70.2 (-CH_2-CH_2-O), 69.67 (-CH_2-O-), and 50.44 (-CH_2-N_3) (Relevant information (Fig. S1D).

2.3.3. Synthesis of PEG Diamine

A reduction method was employed to synthesize PEG Diamine (PEGDA). In a typical synthesis process, PEGD (0.4 g, 0.193 mmol) was dissolved in anhydrous tetrahydrofuran (minimum solubility) followed by gradual addition of triphenylphosphine (0.202 g, 0.772 mmol) to the PEGD solution. The reaction mixture was refluxed at 67°C for 2 h under an inert N_2 atmosphere. After 2 h, distilled water (13 mL) was added to the above mixture and allowed to react for another 10-12 h. A ninhydrin test was performed to confirm the reduction of PEGD to PEGDA. Subsequent confirmation of amine formation, the reaction mixture was evaporated under reduced pressure and extracted with DCM from distilled water. The collected organic layer was evaporated and washed with diethyl ether and hexane several times to remove the negligible quantities of unreacted triphenylphosphine and intermediates of triphenylphosphine (triphenylphosphine oxide). Finally, the obtained product was purified using aluminum oxide column chromatography (mobile phase: 2-30% MeOH and DCM), and the eluted mobile phase was dried under vacuum to obtain a pure form of PEGDA.[29] Thus, synthesized PEGDA was finally characterized and confirmed by ^{1}H NMR and FTIR methods.

The final yield was 93%. ^{1}H NMR ($CDCl_3$, ppm): δ 3.46 – 3.67 (-CH_2-CH_2-O), 2.86 (-CH_2-NH_2), 1.65 (-NH_2) (Fig. S1E). FTMS - probe ESI (m/z): Average mass distribution centered around 2000 for PEG, for PEG diamine, calculatedd-1999.0389 and found-1999.2291 $[M+H]^+$ (Fig. S2B). ΔM= 44.02 Da was observed between two peaks, indicating ethylene glycol (-CH_2-CH_2-O-) fragments.

2.4. Preparation of redox-sensitive polymeric-lipid hybrid nanocarriers

The redox-sensitive polymeric-lipid hybrid nanocarriers (RS-PLHNCs) were fabricated using homogenization and nanoprecipitation methods.[30] Typically, PNIPAM and PEGDA co-polymers were dissolved in 10 mL triple distilled water containing PF-127 as a stabilizer. To the above homogenous aqueous phase, 1 mL of ethanolic lipid solution containing CL-DTDPA, DPPC, stearic acid, and span-80 (75 µL) was added drop-wise under high homogenization. The nanosuspension was further homogenized for another 30 min, followed by gentle stirring until traces of the organic phase were removed. The prepared blank redox nanocarriers (RS-PLHNCs) were further optimized for particle size and stability by varying the composition of excipients used in the aqueous and organic phases during the preparation (given in Table 1). BBR-loaded redox nanocarriers were prepared similarly to the blank nanocarriers, in which BBR was added in the aqueous phase of the nanocarrier preparation.

2.5 Characterization of BBR-loaded RS-PLHNCs

2.5.1. Physical and morphological characterizations of RS-PLHNCs

Prepared nanocarrier formulations were suitably diluted with Milli Q water to determine the average hydrodynamic radius, polydispersity index, and surface charge using Zetasizer (Nano-ZS 90) with a detector angle of 90° at 25°C.[31]

Transmission electron microscope (TEM) was used to evaluate the shape and surface morphology of the optimized RS-PLHNCs. In brief, the BBR loaded nanosuspension was deposited on the copper mesh (TEM grid) by placing 10 µL of sample and incubated for 45 min and negatively stained using 2% uranyl acetate. The prepared sample was dried and visualized under TEM at a voltage of 200kv (Model: JEOL-JEM F200).[30]

2.5.2. Entrapment efficiency (% EE) and drug loading (% DL)

%EE and %DL were determined using dialysis method where BBR-loaded RS-PLHNCs (1 mL) taken in a dialysis bag (10 KDa), was dialyzed in 20 mL of Milli Q water, and allowed

to stand for 1h. The free form of BBR diffused into the milli Q water was quantified at 345 nm using a multi-plate reader (Varioskan Flash, Thermo Scientific).[32]

$$\%EE = \frac{(Total\ drug\ taken - unloaded\ free\ drug)}{Total\ drug\ taken}\ x\ 100$$

$$\%DL = \frac{entrapped\ drug}{weight\ of\ drug\ loaded\ nanocarriers}\ x\ 100$$

2.5.3. ATR-FTIR study

Excipients used in the fabrication of nanocarriers, free form of BBR, blank, and BBR-loaded nanocarriers were evaluated for a shift in the major characteristic functional group during the formulation process using ATR-IR (Bruker-INVENIO R) spectrophotometer.[34] All the spectra were recorded for 32 scans from wavenumber 4000 to 400 cm^{-1} with a resolution of 4 cm^{-1}.

2.5.4. UV-visible spectroscopy

The prepared BBR-loaded RS-PLHNCs and blank nanoparticles (100 µL) were completely dissolved in 900 µL of ethanol and scanned across 250-600 nm using a UV-spectrophotometer (UV BioSpectrometer Kinetic, Eppendorf). The peaks from blank and BBR nanocarriers (BBR NP-**17** & **18**) were compared with free form of BBR to confirm the presence of BBR in the nanocarriers.[33]

2.5.5. Destabilization and characterization of nanocarriers in response to acid and redox stimuli

The pH and redox sensitivity of fabricated nanocarriers were evaluated by the changes in the size, PDI, and zeta potential of nanocarriers on incubation in acidic and reductive environments. In brief, aliquots of RS-PLHNCs were added to the phosphate buffer with four different compositions: (i) phosphate buffer (pH 7.4, 0 mM GSH), (ii) phosphate buffer (pH 7.4, 10 mM GSH), (iii) acetate buffer (pH 4.5, 0 mM GSH), and (iv) acetate buffer (pH 4.5, 10mM GSH). Then, the samples were incubated at 37°C for 24 h with continuous shaking at 100 rpm. After 24 h, samples were analyzed for the modifications observed in morphology by TEM, size, PDI, and zeta potential using a zeta sizer (NanoZS-90).[35]

2.5.6. *In vitro dissolution studies*

In vitro dissolution studies of the fabricated redox nanocarriers were evaluated using the dialysis method in the phosphate buffer pH 7.4 (with and without GSH) and sodium acetate buffer pH 4.5 (with and without GSH).[28,36] Briefly, the optimized BBR-loaded redox-sensitive nanoformulations were placed in a dialysis bag (MWCO 10 KDa) against 20 mL of respective buffer. The samples were incubated at 37°C in a shaking incubator (New Brunswick™ Excella® E24 Shaker Series, Eppendorf) with a rotation speed of 100 rpm. At pre-defined time intervals (0, 1, 2, 4, 8, 12, and 24 h), 0.5 mL of the dissolution medium was withdrawn and replaced with an equal volume of fresh media.[36,37] The BBR concentration in the samples was determined at 345 nm using a plate reader (Varioskan Flash, Thermo Scientific). All the experiments were performed in triplicates, and the data is expressed as mean ± S.D.

The kinetics of the BBR release from the nanocarrier system was further studied by using the following models: zero-order, first-order, Higuchi, Hixson-Crowell, and Korsmeyer-Peppas model.[20]

2.5.7. *Storage and colloidal stability studies*

The stability of the nanoformulation was performed by monitoring the changes in the particle size, PDI, and zeta potential of the different samples stored at 4°C for 6 months.[38]

2.6. In vitro cell-based assays

2.6.1. Cell culture

H1975 (non-small cell lung cancer cells, CRL-5908), HEK293A (normal embryonic kidney cells) and BEAS-2B (normal lung cells, CRL-9609) were cultured in RPMI-1640 medium (Himedia) supplemented with 10% (v/v) FBS (Gibco) and 1% (v/v) penicillin-streptomycin antibiotics (Himedia) and maintained in a humidified CO_2 incubator at 37°C ± 0.2°C and 5% CO_2.

2.6.2. Intracellular GSH estimation

Intracellular GSH levels for H1975, BEAS-2B, and HEK293A were initially determined (in 1 × 10^6 cells) following 3-4 times wash with ice-cold phosphate buffer saline (PBS) and centrifugation at 3000g for 10 min at 4°C. The pellet was resuspended in 300 µL of extraction buffer and sonicated for 5 min using a probe sonicator at cold temperature (30% amplitude, 5-sec pulse ON and 5 sec OFF). Later, the mixture was centrifuged to remove the

precipitated proteins, and the supernatant was used for GSH estimation using Ellman's reagent (DTNB reagent: Sigma). Finally, 20 µL of the supernatant was mixed with 20 µL of KPE buffer, and the homogenous solution was added with 120 µL of Ellman's reagent, and the absorbance was measured at 412 nm. The intracellular GSH was calculated from the standard GSH calibration curve.[39]

2.6.3. Biocompatibility and in vitro redox-sensitive cytotoxicity study

The redox-sensitive cytotoxicity of the fabricated nanocarriers was determined in BEAS-2B, HEK293A, and H1975 cells. Prior to the assay, 1×10^4 cells/well were seeded in 96-well plate and cultured for 24 h to ensure cell adherence.[40] The cells were treated with different concentrations (3.125 to 50 µM BBR) of redox-sensitive BBR-loaded nanocarriers (batch **17** and **18**), free form of BBR, blank nanocarriers, and control groups. After 24 h and 72 h treatment, the culture medium was replaced with 30 µL of MTT (Himedia) in PBS (5 mg/mL) in each well and allowed to incubate for 4 h in a CO_2 incubator at 37°C and 5 % CO_2. The MTT solution was removed, and 150 µL of DMSO was added to each well to dissolve MTT-Formazan crystals. The intensity of the purple color from the wells was measured at 570 nm to determine the %cell viability. The cytotoxicity induced by the BBR-loaded redox nanocarriers in H1975 lung cancer cells was compared with BEAS-2B and HEK293A normal cells to evaluate the redox-responsive cytotoxicity. BBR-loaded RS-PLHNCs induced cytotoxicity was compared with the free form of BBR in H1975 cancer cells to confirm enhancement in cell killing efficiency.

2.6.4. Estimation of cytotoxicity of the nanoparticles

The effect of nanoparticles on cell viability was studied using the standard MTT assay. H1975 cells (1×10^6 cells/well) were seeded in 6-well plates. Following overnight incubation (37°C in a 5% CO_2) and cellular adherence, nanoparticles were added into the culture media at corresponding IC_{50} values (from MTT assay) and were further incubated for 24 h. Non-adherent dead cells were removed by gentle washing with PBS. The adherent live cells from the plate were harvested by trypsinization (trypsin-EDTA solution, Himedia), washed, and diluted with PBS buffer. The viable cell population was counted (using a hemocytometer) following the standard protocol. The experiments were performed in triplicates and repeated on two independent events to ensure reproducibility and reliability.[41]

2.6.5 Estimation of GSH content following BBR and BBR-loaded nanoparticulate treatment

About 5×10^5 H1975 cells/well were seeded in a 6-well plate and incubated for 24 h. The cells were treated with free form of BBR, and nanoparticulate-loaded BBR (BBR NP-**17** and **18**), at the respective IC_{50} values of BBR nanocarriers determined in the MTT assay. Post-treatment, the GSH levels were determined following the protocol for GSH estimation provided in **section 2.6.2**.

2.6.6 In vitro cellular uptake studies

Cellular uptake of prepared nanocarriers was performed using confocal laser scanning microscopy (CLSM; Leica model) and flow cytometry (FACS; Calibur BD LSR Fortessa TM).

2.6.6.1 Flow cytometry (quantitative analysis)

The cellular uptake of free form of BBR or nanoformulation was quantified by flow cytometry.[42] H1975, BEAS-2B, and HEK293A cells (1×10^6 cells/well) were seeded in a 6-well plate and incubated for 24 h at 37°C under 5% CO_2. Following cell adherence, the BBR nanoparticles and free form of BBR were added to the corresponding wells (at IC_{50} values equivalent to BBR nanoparticles) and incubated for 4 h, 12 h, and 18 h. Following incubation, the cells were washed with ice-cold PBS (3 times), harvested, and centrifuged at 3000g for 10 min. Finally, the cells in each sample were resuspended in 400 µL PBS for FACS analysis. The cellular uptake of BBR was quantified using the fluorescence mean intensity by gating 10,000 cells (n=3) (λ_{ex} = 488 nm and λ_{em} = 585 nm).

2.6.6.2 Confocal Laser Scanning Microscopy (CLSM)

CLSM was used to analyze the intracellular distribution of free form of BBR, BBR-loaded RS-PLHNCs, and blank nanocarriers.[43] H1975 lung cancer cells, BEAS-2B normal lung cells and HEK293A normal embryonic kidney cells (1×10^5 cells/well) were seeded on a cover slip. Post 24 h incubation, the formulations/free form of BBR were added to cells with the determined IC_{50} values respective to BBR nanoparticles and incubated for 4 h and 18 h with PBS as a control. Post-treatment, the cells were washed (3x) with ice-cold PBS and fixed with 4% w/v paraformaldehyde. The cells were mounted onto glass slides using FlouroG mount media (Invitrogen) and observed under CLSM (λ_{ex} = 405 nm and λ_{em} = 550 ± 50 nm).

2.6.7 Apoptosis study

2.6.7.1 Apoptosis study by flow cytometry

To study apoptosis, BEAS-2B, HEK293A, and H1975 cells were seeded in a 6-well plate with 1×10^6 cell density and incubated at 37°C under 5%CO_2 incubator for 24 h. After adherence, cells were treated with IC_{50} values of BBR-loaded nanocarrier (BBR NP-**17** & NP-**18**), free form of BBR (FR-**17** & FR-**18**), blank nanoparticulate (BLK NP-**17** & BLK NP-**18**) for 4, 12, and 18 h. After treatment, cells were collected and washed twice with cold PBS then centrifuged at 1500rpm for 5min at 4°C. The resulting pellet was resuspended in 1X binding buffer containing 5 µL each of fluorescein isothiocyanate (FITC)-labeled Annexin V (λ_{ex} = 488 nm and λ_{em} = 518 nm) and propidium iodide (PI) (λ_{ex} = 561 nm and λ_{em} = 616 nm) for 20 min in dark condition at room temperature. Finally, stained cells were detected in flow cytometer with 10^4 gating cells. In the apoptosis dot plot, Q1 (Annexin V-FITC-/PI+) indicates necrosis, Q3 (Annexin V-FITC-/PI-) normal live cell population whereas, Q2 (Annexin V-FITC+/PI+) and Q4 (Annexin V-FITC+/PI-) represents late and early apoptosis respectively (Fig. S10). The BD FACSDivaTM software determined the % apoptotic cells.[40] The assay was performed in triplicates.

2.6.7.2 Annexin V staining for apoptosis

CLSM was used to analyze the apoptotic cells stained with Annexin V-FITC upon free form of BBR, BBR-loaded RS-PLHNCs, and blank nanocarriers treatments.[43] H1975 lung cancer cells, BEAS-2B, HEK293A, and H1975 cells were seeded with 1×10^5 cells/well density on a cover slip. Post 24 h incubation, the formulations/free form of BBR were added to cells with the determined IC_{50} values respective to BBR nanoparticles and incubated for 4 h and 18 h with PBS as a control. Post-treatment, the cells were washed (3x) with ice-cold PBS and stained with Annexin V-FITC for 15 min in dark condition at room temperature. After staining, the cells was fixed with 4% w/v paraformaldehyde and the coverslips were mounted onto glass slides using FlouroG mount media (Invitrogen) and observed under CLSM (λ_{ex} = 488 nm and λ_{em} = 550 ± 50 nm).

2.6.7. Gene Expression Studies

2.6.7.1. RNA isolation

In seven groups, RNA was isolated from H1975 cells (1×10^6 cells/well) treated with IC_{50} values of BBR-loaded nanocarrier (BBR NP-**17** & NP-**18**), free form of BBR (FR-**17** & FR-**18**), blank nanoparticulate (BLK NP-**17** & BLK NP-**18**). Post 24 h, cell pellets were harvested and resuspended in Trizol (500 µL, Invitrogen). Then, 0.2 mL of chloroform was

added into the suspension and vortexed vigorously under ice-cold conditions. The cell suspension was centrifuged at 12,000 × g; 4°C for 15 min; the supernatant (aqueous phase) was further aspirated carefully and transferred into a fresh tube. 500 µL of isopropanol was added to the supernatant, incubated for 10 min, and centrifuged at 12,000 × g for 10 min at 4°C. Further, the pellet was washed with 75% ethanol by centrifuging at 12,000 × g for 10 min at 4°C. The obtained RNA pellet was air-dried and dissolved in 20 µL of DEPC-treated nuclease-free water. The concentration and purity of RNA was estimated by NanoDrop (ONE^{C}, Thermo Fisher Scientific), and quality was checked by 1% agarose gel electrophoresis. Good quality of RNA (260/280 ratio = 1.9 - 2.0) with two visible bands was considered for cDNA synthesis. For reverse transcription, 2 µg of total RNA was used through the Reverse Transcription Kit (Maxima First Strand cDNA kit, Thermo Fisher Scientific) in a Thermal Cycler (Veriti, Applied Biosystems) following the manufacturer's instructions.

2.6.7.2. Quantitative Reverse Transcription Polymerase Chain Reaction (qRT-PCR) Study

Real-time PCR study was performed to measure the mRNA expression levels of PUMA, NOXA, MCL-1, NFE2L2, NQO1, TXRND1, HMOX1, and GAPDH (housekeeping gene) using iTaq universal SYBR green supermix (Biorad) in QuantStudio5 (Applied Biosystems). 2 µL of prepared cDNA was used for 10 µL reaction, with 5 µL of SYBR, 1 µL of nuclease-free water, and 1µl (0.25 µM) of forward and reverse primer each. PCR reaction was performed with the following temperature cycle: Initial denaturation (95°C for 20 sec), 40 amplification cycles (denaturation at 95°C, 3 sec; annealing at 60°C, 30 sec). The fold change of target mRNA was calculated using $2^{-\Delta\Delta Ct}$ values obtained from treated samples when compared with control samples. The forward and reverse primer sequences used are listed in Table S2.

2.7. Statistical analysis

All data were normalized to the control values of each assay and expressed as mean ± SEM. Statistical analysis was performed using one-way ANOVA followed by Dunnett's multiple comparison test for comparative analysis between multiple groups and two-way ANOVA followed by Turkey's multiple comparison test between multiple groups with two or more independent variables utilizing GraphPad Prism 8.0 (GraphPad Software, La Jolla, CA, USA). p values: *p<0.05, **p< 0.01, ***p<0.001, ****p<0.0001 were considered statistically significant.

3. Results and discussion

3.1 Synthesis and characterization of redox-cholesterol (CL-DTDPA) and aminated polyethylene glycol (PEGDA)

A hydrophobic dual-responsive compound, redox-cholesterol (CL-S-S-COOH, **CL-DTDPA**), was prepared by modifying CL with a disulfide-containing monomer (DTPA) *via* an esterification reaction, as shown in Scheme 1A. From ^{1}H NMR (Fig. 1A) spectra, three triplet peaks between 2.6 – 3.0 ppm confirmed DTDPA conjugation to CL. The peaks from ^{13}C NMR spectra (Fig. 1B), at 177.9 ppm for carboxylic acid (C=O) and 171 ppm for ester C=O, also confirmed the DTDPA conjugation. From FTIR, the conserved characteristic peaks of CL and DTPA, a peak shift from 1687 to 1729 cm^{-1} indicating the conversion of carboxylic acid to an ester functional group further verified the synthesized conjugate (Fig. 1C). From both NMR and FTIR studies, the synthesis of **CL-DTDPA** was confirmed.

The hydrophilic PEG diamine (**PEGDA**) was synthesized by step-by-step conversion of PEG to di-tosylated PEG (PEG-OTs), later to PEG diazide (PEG-N_3), and finally to PEG diamine (PEG-NH_2) (Scheme 1B). The PEG-OTs formation was confirmed by ^{1}H NMR and ^{13}C NMR (Fig. S1A & S1B). The two doublet peaks corresponding to benzene protons at 7.77 ppm and 7.48 ppm and the carbon peaks between 125 – 146 ppm confirm the PEG-OTs conversion. The absence of benzene peaks in ^{1}H (Fig. S1C) and ^{13}C (Fig. S1D) NMR spectra indicated PEG azide formation. A shift in triplet peak from 3.37 ppm (-CH_2- adjacent to azide) to 2.86 ppm (-CH_2- adjacent to amine) indicated PEGD conversion to PEGDA (Fig. S1E). Moreover, the FTIR peak (Fig. S1F) at 3446 cm^{-1}, corresponding to N-H symmetrical and asymmetrical stretching of primary amine groups was present only in PEGDA (absent in PEGD)[44,45]. NMR and FTIR data confirmed a successful synthesis of PEG diamine (PEGDA).

Thus, redox-cholesterol (CL-DTDPA) and PEG diamine (PEGDA) were synthesized and characterized to fabricate the BBR-loaded redox-sensitive PLHNCs.

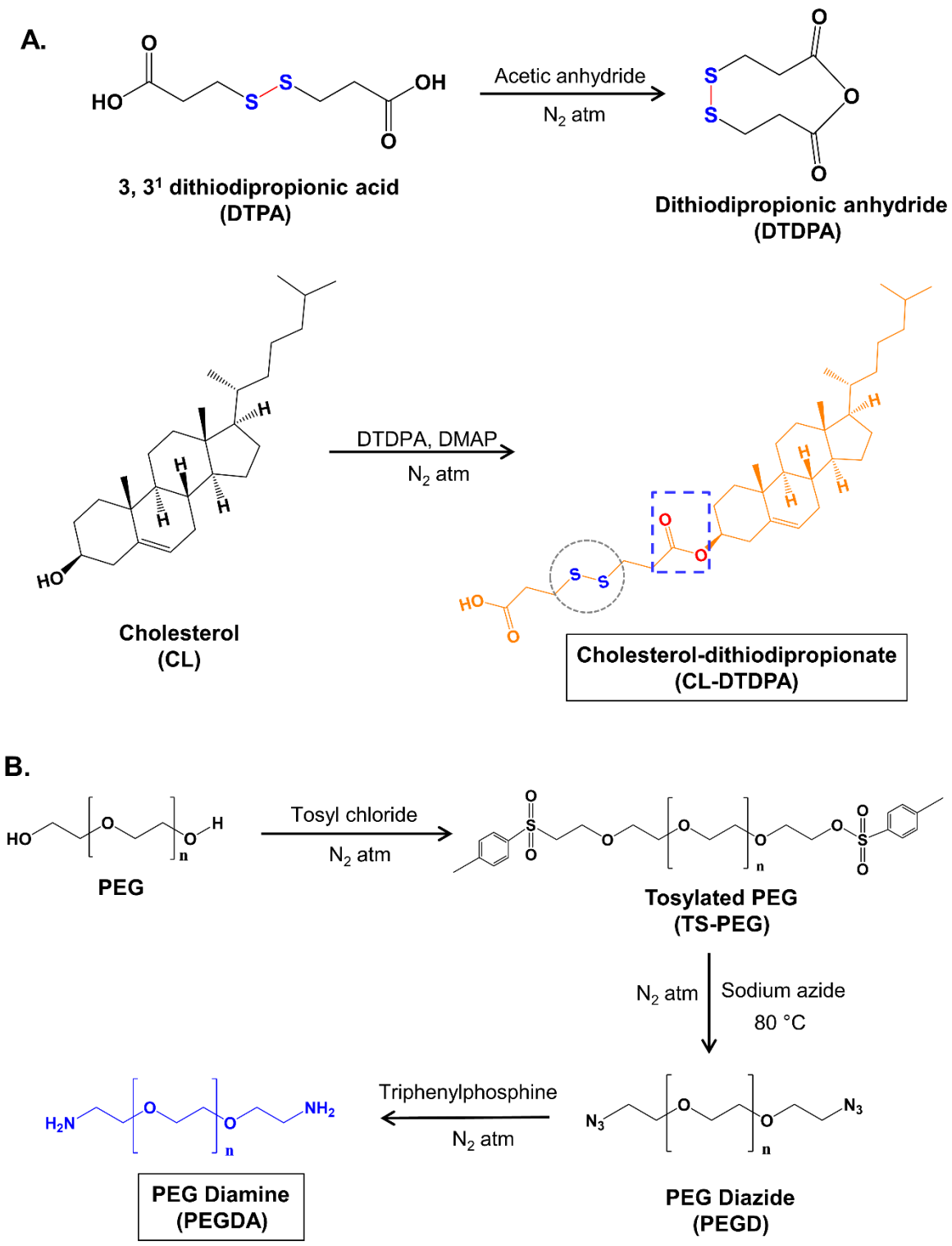

Scheme 1. Synthetic schemes of Cholesterol-Dithiodipropionate (redox-sensitive cholesterol) (A) and PEG diamine (B)

483

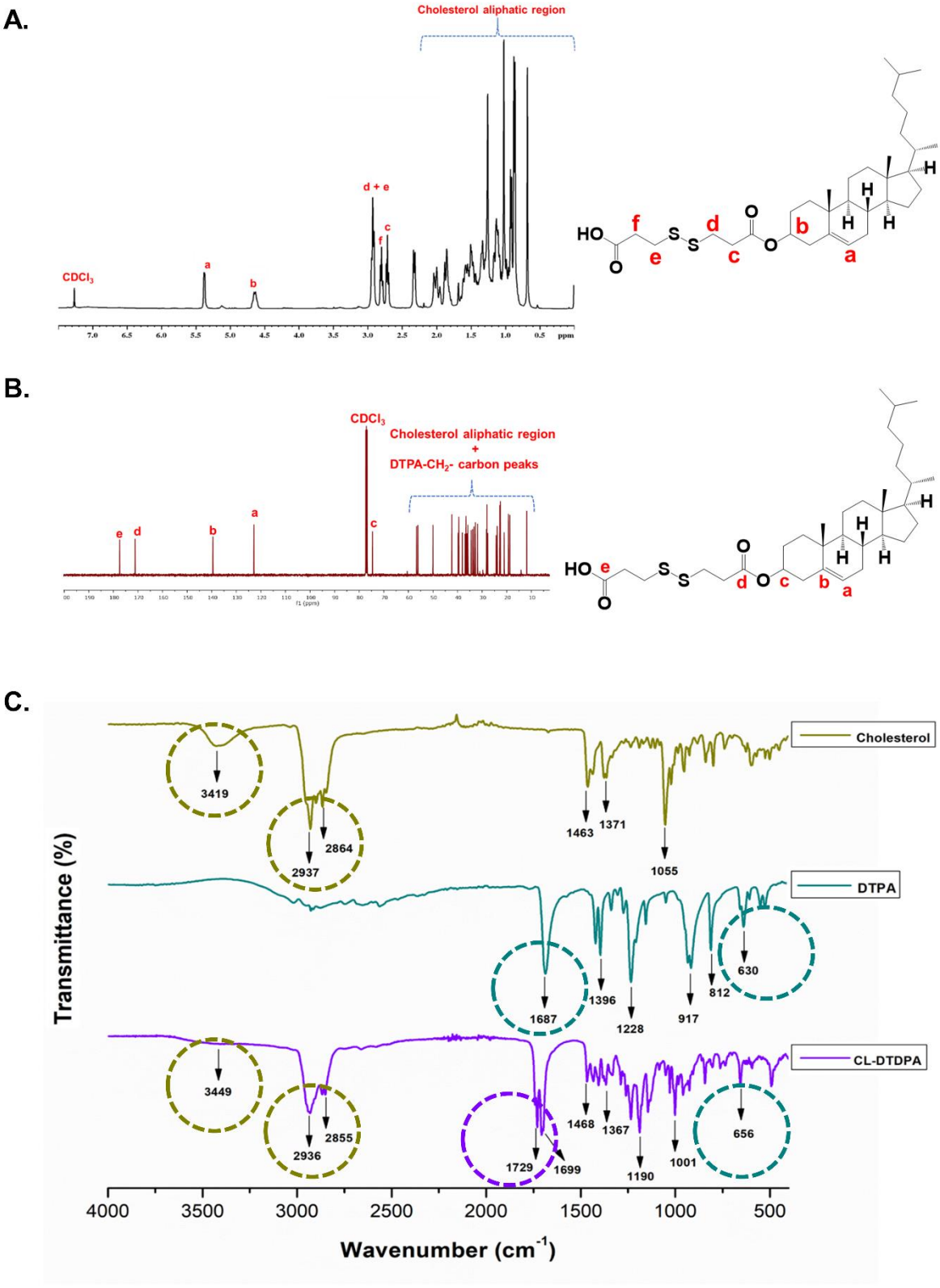

Fig. 1. ^{1}H NMR (A), ^{13}C NMR (B), and FTIR (C) of Cholesterol-Dithiodipropionate (CL-DTDPA)

484

3.2. Fabrication and characterization of berberine-loaded redox-sensitive PLHNCs (BBR-loaded RS-PLHNCs)

In the current work, homogenization and nanoprecipitation methods were employed to fabricate stable homogeneous **BBR-loaded RS-PLHNCs** with a diameter < 200 nm and PDI of 0.25.[46] The fabricated nanocarriers comprise a drug-embedded polymer core layer encased by the redox lipid to prevent premature drug release under physiological conditions. From a preliminary study, blank nanocarriers of different polymer and lipid compositions were prepared to obtain a nanoformulation of optimal particle size, uniformity, and stability (as shown in Table 1). Among the eight batches, batch **#3** and **#7** had good stability, relatively less particle size, and homogenously distributed. Batch **#7**, containing stearic acid, displayed a larger particle size than batch **#3**, as it increased the lipid matrix's thickness and thereby increased the overall particle's hydrodynamic radius. In all batches with stearic acid, span-80 surfactant with higher lipophilicity (HLB value 4.3) was preferred over tween-80 for nanocarrier stabilization as it facilitated the miscibility of highly lipophilic stearic acid in the aqueous phase by reducing the interfacial tension between the aqueous and lipid phase.

Table 1 Preliminary study on the effect of various excipients on particle size and its distribution

Batch no #	**Redox-Cholesterol (mg)**	**Stearic acid (mg)**	**DPPC (mg)**	**PNIPAM (mg)**	**BBR (mg)**	**PS (nm)**	**PDI**
1	15	10	10	20	-	212±1.29	0.15±0.01
2	15	10	10	-	-	246±1.48	0.17±0.04
3**	15	-	10	20	-	151±2.82**	0.12±0.03**
4	15	10	-	20	-	233±3.36	0.25±0.01
5	20	10	10	20	-	236±3.37	0.26±0.03
6	15	20	10	20	-	314±9.22	0.36±0.06
7***	15	10	20	20	-	210±4.59***	0.18±0.05***
8	20	20	20	20	-	222±0.64	0.25±0.03
Composition for fabrication of berberine-loaded redox-sensitive PLHNCs (BBR-loaded RS-PLHNCs)							
17** BBR NP-**17**	15	-	20	20	1	125±1.21**	0.15±0.02**
18*** BBR NP-**18**	15	10	20	20	1	185±1.56**	0.15±0.02***
Constants							
PEGDA-20 mg and PF-127-100 mg							

Finally, the compositions of batches **#3** and **#7** in preparing blank nanocarriers (BLK NPs) were utilized to fabricate **BBR-loaded RS-PLHNCs** (Batch **17** and **18**), with minor changes in the composition. In BBR NP-**17**, the amount of DPPC was increased from 10 to 20 mg to

equally maintain the DPPC concentration in BBR NP-**18** to examine further the influence of stearic acid on physicochemical characteristics and stability of the nanocarrier. The optimized BBR-loaded RS-PLHNCs showed %EE and %DL of 90.52 ± 4.68 and 1.12 ± 0.06 in BBR NP-**17** and 95.42 ± 3.51 and 1.05 ± 0.05 in BBR NP-**18** respectively. The increased encapsulation of BBR in BBR NP-**18** is ascribed to the presence of lipophilic stearic acid in the lipid matrix, which may increase the protection of the polymeric layer in which the drug was embedded and further prevent the leakage of the drug into the dispersion phase than the BBR NP-**17**.

The optimized nanoformulations (BBR NP-**17** and **18**) exhibited nearly spherical shaped uniform nanosized particles (Fig. 2A and B). The appearing bright portions in the image might indicate the presence of polymeric core, while thin lining was observed around the periphery of the core which would be of a lipid shell coating. During the evaporation process in the nanocarrier synthesis, the polymer might form the core entrapping the drug and lipids might self-assemble surrounding the polymeric core.[47] These spherical particles of BBR NP-**17** and **18** showed average particle size of 124.7 ± 1.21 and 185.17 ± 1.56 nm and PDI of 0.153 ± 0.02 and 0.152 ± 0.02, respectively using dynamic light scattering (DLS). Alongside the particle size, both formulations exhibited negative zeta potential (-5.91 ± 2.54 and -20.03 ± 1.07 mV) due to the coating of negatively charged lipid matrix (DPPC, stearic acid, and CL-DTDPA mixture) on the surface of the polymer core (Fig. 2A and 2B).[48] These features are essential for particle retention and uptake by EPR in cancer cells for its activity.

FTIR was performed to analyze the incorporation of BBR in the nanocarrier system and to detect for incompatibilities/interactions between the BBR and excipients or among the excipients used in the formulation (Fig. 2C and Fig. S3B). From the FTIR data, primary absorption peaks of free form of BBR were observed at 3209 cm^{-1} (–OH stretching vibration of methoxy group), 2906 and 2852 cm^{-1} (–CH stretching vibration), 1632 cm^{-1} (–C-N stretching vibration), 1505 cm^{-1} (–C=C stretching vibration) and 1102 cm^{-1} (–C-O-C stretching vibration).[22,49,50] Comparing the FTIR spectra of free form of BBR, physical mixture, BLK NPs, and BBR NPs (summarized in Table 2), no new characteristic peaks were detected. Only negligible shifts in the characteristic peaks were noted between them, suggesting the association of weak interactions between the drug and excipients. In BBR NPs, BBR-specific characteristic peaks were not clearly distinguished. This may be due to the overlapping of peaks with the excipients or BBR incorporated into the polymer core, whose characteristic peak intensities may be negligible. This data confirms no potential

chemical interactions between drug and excipients or among the excipients. However, the incorporation of BBR into the nanocarrier system was not clearly addressed. Therefore, we performed a UV spectroscopy based study to confirm the loading of BBR in the nanocarrier system.

UV spectroscopy data displayed characteristic peaks for BBR incorporated in BBR NP-**17** and NP-**18** at 260 nm (peak A), 345 nm (peak B), and 424 nm (peak C) wavelengths, which were similar in comparison to free form of BBR, while no peaks were observed in BLK NP-**17** and **18** (Fig. S3A). The results from both UV and FTIR spectra confirmed the successful encapsulation of BBR into the redox nanocarrier system without any specific covalent modifications/interactions.

Table 2 FTIR spectra characteristic peaks and their respective functional groups in different samples

	Characteristic peak (Wavenumber cm^{-1})					
Free form of BBR (i)	3209	2906, 2852	-	1632	1505	1102
Functional group (i)	Intermolecular -OH (methoxy group	-CH stretching		–C-N stretching	–C=C stretching	-C-O-C stretching
Physical mixture (ii)	3340	2885	1729	1640	1552	1102
BLK NPs (iii)	3369	2885	1732	1644	1552	1097
BBR NPs (iv)	3360	2885	1737	1644	1547	1102
Functional group (ii), (iii) and (iv)	-OH stretching	-CH stretching	-C=O stretching (ester or acid)	-C=O stretching (amide group)	-NH bending (amide group)	-C-O-C stretching
Inference	PF-127 / DPPC/ CL-S-S-COOH / PNIPAM	(ii) and (iii) PNIPAM / PF-127/ PEGDA / CL-S-S-COOH / DPPC / stearic acid (iv) **BBR**/ PNIPAM / PF-127/ PEGDA / CL-S-S-COOH / DPPC / stearic acid	CL-S-S-COOH / DPPC	PNIPAM	PNIPAM	(ii) PF-127 / PEG diamine / DPPC (iv) **BBR**/ PF-127 / PEG diamine / DPPC

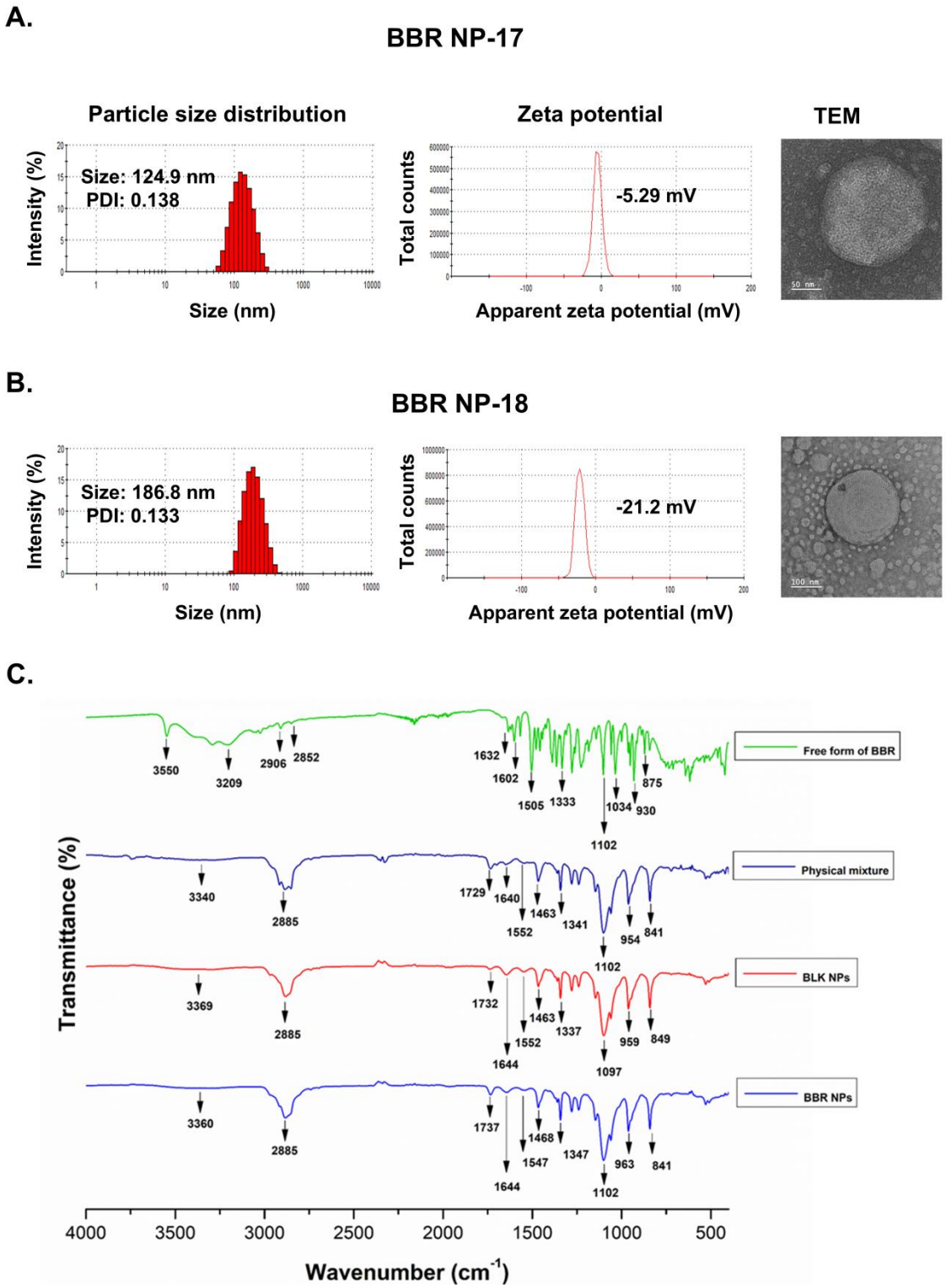

Fig. 2. Characterization of BBR-loaded redox-sensitive PLHNCs. TEM images represent the morphology of the fabricated nanoparticles and DLS graphs illustrate the particle size, PDI, and zeta potential of BBR NP-**17** and **18** (A) and (B). FTIR spectra of free form of BBR, blank, and BBR-loaded NPs (C).

552

3.3 Reduction-triggered nanocarrier disassembly and BBR release from the nanocarriers

Redox/pH-sensitive behaviors of the optimized nanocarriers (BBR NP-**17** and BBR NP-**18**) were studied by observing the changes in the morphology, particle size and distribution of nanocarriers in tumor microenvironment simulated conditions. L-Glutathione (GSH, 10mM) was used as a simulant for reductive microenvironment[51,52] and a pH of 4.5-5.0 to mimic the intracellular endo-lysosomal acidic microenvironment, as these are the crucial parameters that prevail in the tumor microenvironment.[53] Following 24 h incubation in pH 7.4 with 10mM GSH buffer, DLS data presented significant increase in the hydrodynamic radius in both batches from 125.8 ± 0.7 to 321.1 ± 8.7 nm (BBR NP-**17**) and 195.4 ± 1.9 to 381.2 ± 7.3 nm (BBR NP-**18**) in pH 7.4 with 10mM GSH buffer, while no remarkable changes in particle size were evidenced in pH 7.4 without GSH condition (Fig. 3A (i) and B (i)). Additionally, aggregation of nanocarriers with alteration in the shape was observed using TEM, while no morphological changes were displayed in the nanocarriers incubated in pH 7.4 buffer without GSH (Fig. 3A (ii) and 3B (ii)). Similarly, BBR NP-**17** and BBR NP-**18** had a non-homogenous particle distribution (with higher PDI values of 0.22 ± 0.014 to 0.48 ± 0.02 and 0.16 ± 0.01 to 0.4 ± 0.03, respectively) in GSH environment, while negligible deviations were observed in normal conditions. These changes were mainly attributed to the reduction and cleavage of disulfide bonds (-S-S-) present in the redox-cholesterol (CL-S-S-COOH) that destabilized the lipid matrix coated on the surface of the polymer core.[54,55] Similarly, the pH responsiveness of nanocarriers upon exposure to acidic pH (pH 4.5) displayed increased aggregation and complete change in the shape of the nanocarriers with substantial increase in particle size to 457.8 ± 30 nm (BBR NP-**17**) and 315.6 ± 10.4 nm (BBR NP-**18**) and PDI to 0.55 ± 0.01 (BBR NP-**17**) and 0.53 ± 0.04 (BBR NP-**18**), which was ascribed due to the hydrolysis of ester bonds in acidic pH (Fig. 3A (i) and B (i)).[56,57] Analogous results with morphology, larger particle size and PDI were observed in the combination of pH and reduction dual stimuli (Fig. 3A (ii) and B (ii)). On the contrary, only a slight decrease in the zeta potential was observed in all the exposure conditions.

In vitro BBR release

BBR release behavior from the RS-PLHNCs was evaluated in simulated tumor microenvironment and normal physiological conditions. At normal physiological conditions (pH 7.4, 0mM GSH), about 48.7% of the drug was released from batch **17** and 36.3% from

batch **18** in 24 h. Interestingly, both nanocarriers exhibited a significant increase in the rate of drug release in the presence of 10mM GSH (40-50% of BBR release within 2 h) that further sustained to 93-94% at 24 h respectively (shown in Fig. 4A and B) compared to normal physiological conditions. This burst release of BBR is accredited to the specific cleavage of disulfide bonds present in the redox-cholesterol (CL-S-S-COOH) in the reductive environment (GSH), while only diffused controlled release occurred at pH 7.4 due to non-cleavage of the redox and pH-sensitive bonds in the nanocarriers. This hypothesis is consistent with the reduction-triggered nanocarrier disassembly study (Fig. 3), where the increase in the particle size and PDI of the nanosuspension was observed in response to the GSH environment (10mM GSH).

Further, these BBR-loaded RS-PLHNCs were evaluated for drug release at lysosomal pH (pH 4.5) and complete tumor intracellular microenvironment (pH 4.5 and GSH). At pH 4.5, with and without GSH, a burst release of BBR with >50% release within 2 h and >80% release within 4 h in BBR NP-**17** and 8 h in BBR NP-**18** was observed. At pH 4.5, the observed accelerated release may be due to the hydrolysis of ester bonds present in the redox cholesterol (ester linkage between CL and DTPA) and further destabilization of the nanocarriers followed by the release of BBR.[58] A remarkable rapid release of nanocarriers was observed in both acidic and GSH conditions that triggered the cleavage of dual stimuli of nanocarriers (i.e., disulfide bonds in response to GSH redox stimuli and ester linkages to acidic pH stimuli) constituted to increased release. (Fig. 4A and B)

In all dissolution media, BBR NP-**18** showed a significant, sustained BBR release rate in comparison to BBR NP-**17** due to the presence of stearic acid in the lipid composition that increased the lipophilicity and mechanical strength of the nanocarrier system, resulting in decreased diffusion of drug from the nanocarrier system.

Mechanism of the BBR release from nanocarriers

From the BBR release kinetics data, a Higuchi model of BBR release behavior was predominantly observed from RS-PLHNCs, except under pH 7.4 in addition to 10 mM GSH, where the Hixson-Crowell model was followed (Table S1 and Fig. S4). According to the Higuchi model, BBR release may occur via diffusion from the nanocarrier system or through lipid and polymer matrix erosion.[30,59] Conversely, the Hixson-Crowell model suggests that the nanoparticles released the drug by changing the surface area or diameter of the nanocarrier system.[60] This implies that the nanocarriers incubated in a reducing environment

experience changes in the surface area or diameter of the nanocarriers by cleavage of the disulfide bonds and facilitate BBR release simultaneously into the dissolution media.

In summary, the experimental findings indicate that BBR release from RS-PLHNCs is influenced by a combination of diffusion and erosion mechanisms, with the release behavior being affected by microenvironmental factors such as pH and the presence of reducing agents like GSH.

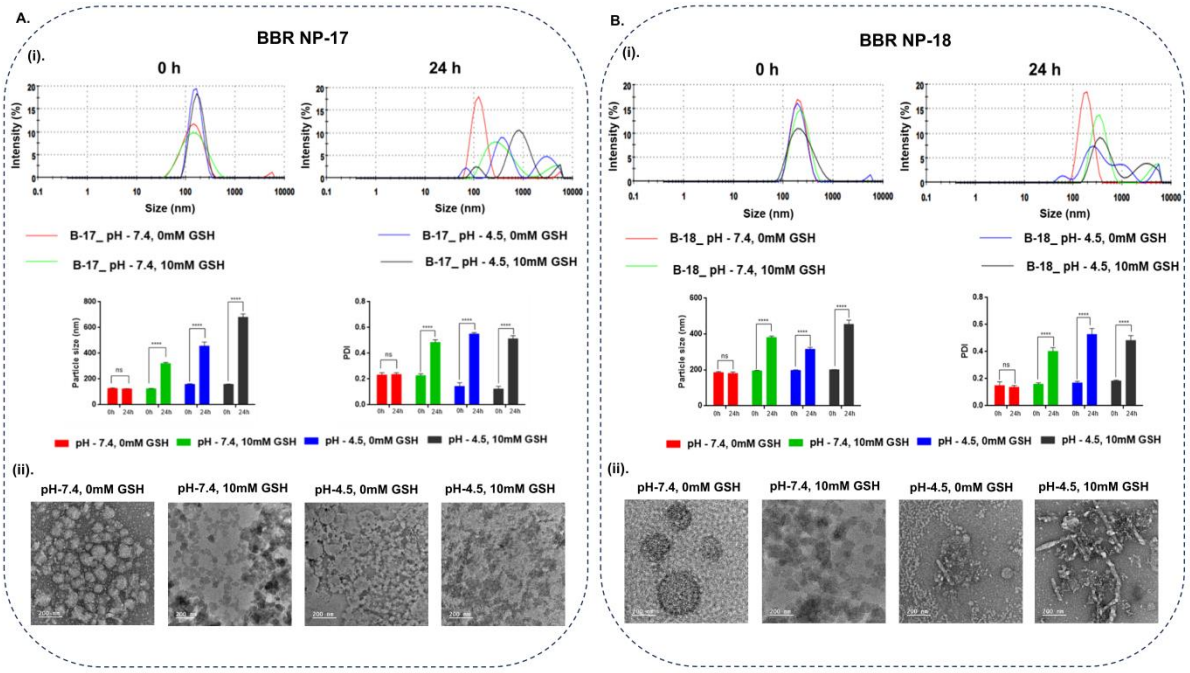

Fig. 3. Redox-responsive study of BBR NP-**17** (A) and BBR NP-**18** (B) in normal and tumor-simulated conditions. Particle size distribution and their respective graphs of both nanoparticles after incubation at 0 and 24 h in normal physiological and tumor-simulated conditions (A (i) and B (i)). Data is presented as mean ± S.D, (n=3). A two-way ANOVA was used to compare the deviations in the particle size and PDI of the nanocarriers in normal and tumor-simulated conditions. Differences in p values, *p<0.05, **p<0.01, ***p<0.001, ****p<0.0001, were considered statistically significant and ns was considered non-significant. TEM images of BBR NP-**17** and **18** (A (ii) and B (ii)) after incubation at 0 and 24 h in normal physiological and tumor-simulated conditions, illustrating changes in nanoparticle morphology and aggregation in response to the redox-sensitive environment.

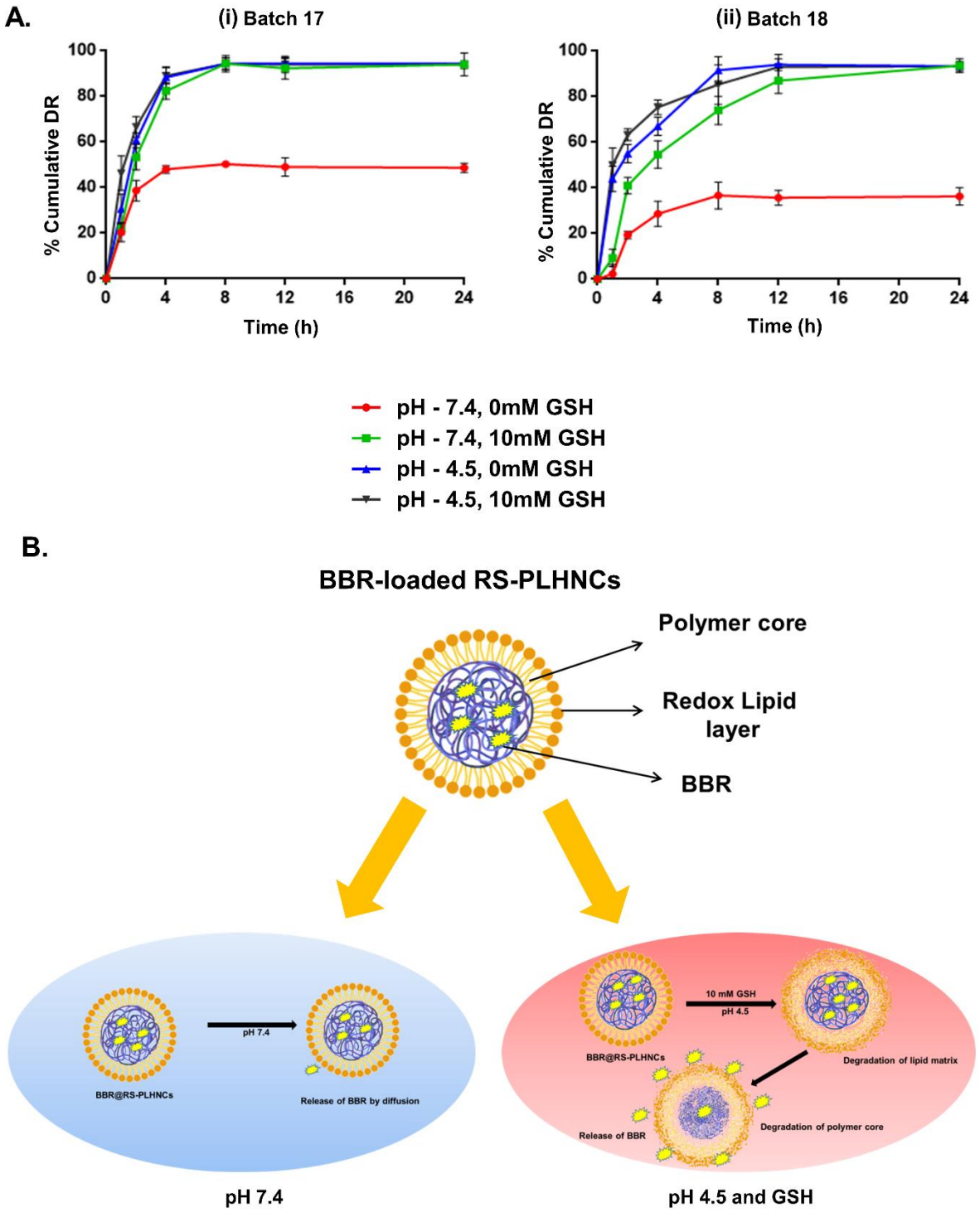

Fig. 4. *In vitro* release studies. Graphical representation of dissolution studies in normal physiological (pH 7.4 buffer, without GSH) and simulated TME (pH 7.4 with 10 mM GSH, pH 4.5 and pH 4.5 with 10 mM GSH) for BBR NP-**17** and NP-**18** (A (i and ii)) (data is represented as mean ± S.D, n = 3). Schematic representation of drug release from the redox-sensitive nanocarriers under normal and simulated TME (B).

623

3.4 Storage and colloidal stability studies

Stability studies are performed to assess the storage-related conditions of the prepared nanoformulation for long-term usage. In this study, stability assessments were conducted for 180 days at 4°C. The optimized BBR-loaded nanocarriers (BBR NP-**17** and **18**) showed free of aggregation or precipitation with only negligible changes in the particle size and distribution during the initial 60-day storage period. Extending the study to 180 days revealed contrasting behaviors: BBR NP-**17** showed reduced homogeneity and increased particle size, whereas batch **18** demonstrated increased uniformity and size, indicating superior colloidal stability and dispersion (Table 3 and Fig. S5). The decreased stability of the BBR NP-**17** might be due to the zeta potential value being near zero. In contrast, the zeta potential of batch **18** is > -20 mV, contributing to good steric repulsion and colloidal stability. Previous studies suggest that nanocarriers aggregate with lower zeta potential due to reduced steric repulsion between particles.[32] The higher negative charge of nanoparticles in batch **18** could be attributed to the addition of stearic acid having carboxylic groups, contributing to good physical stability during storage.

Table 3 Storage stability studies of the BBR-loaded RS-PLHNCs for 180 days at 4°C

	BBR NP-17		
Time (days)	**Particle size (nm)**	**PDI**	**ZP (mV)**
0	124.7±1.2	0.153±0.02	-5.91±2.54
60	156.7±1.7	0.146±0.03	-5.73±0.68
180	173.2±4.7	0.366±0.06	-2.68±0.43
	BBR NP-18		
0	185.2±1.6	0.153±0.02	-20.03±1.07
60	171.3±0.8	0.120±0.01	-23.93±1.1
180	177.7±2.2	0.139±0.03	-25.63±4.29

3.5. In vitro cell-based assays

The redox sensitivity hypothesis of the BBR-loaded RS-PLHNCs was validated by investigating the specific killing efficiency of the synthesized BBR-loaded RS-PLHNCs in both normal cells (with lower GSH) and cancer cells (with higher GSH). For this purpose, normal (BEAS-2B & HEK293A) and cancer (H1975) cells were chosen to evaluate the redox sensitivity and therapeutic killing efficiency of the fabricated BBR-loaded NPs and compared to free form of BBR.

3.5.1. Intracellular GSH estimation

Due to the disparity in GSH levels among cancer versus normal cells, the levels aimed to elucidate further their potential implications in the cellular response to specific BBR release and subsequent selective cytotoxicity. Analysis revealed substantial elevated levels of GSH in H1975 cancer cells, exhibiting ~11 and 3.82-folds increased concentrations compared to BEAS-2B and HEK293A cells respectively. Specifically, GSH concentrations were quantified to be 238.28 ± 2.8 µM in H1975 cancer cells, 21.55 ± 3.17 µM in BEAS-2B and 62.24 ± 2.12 µM in HEK293A cells (Fig.S6.A). These findings underscore the suitability of both cell lines for validating the proposed hypothesis concerning selective BBR release and subsequent preferential cell death based on GSH levels.

3.5.2. In vitro cytotoxicity studies

Redox-responsive cytotoxicity

The cytotoxic effects of free form of BBR, BBR NP-**17**, and BBR NP-**18** were evaluated by MTT assay in BEAS-2B, HEK293A, and H1975 cells. As depicted in Fig. 5A and B, all three formulations exhibited dose-dependent inhibitory effects in both cell lines. IC_{50} values of the respective formulations were reported in Table 4 and Fig S6 (B (i & ii).

In terms of redox sensitivity (Fig 5A i & iii)), BBR-loaded RS-PLHNCs (BBR NP-**17** and **18**) displayed significant cytotoxicity effects at all concentrations except 3.125 µM at 24 h in H1975 cancer cells compared to BEAS-2B cells. After 72 h incubation (Fig 5A, ii & iv), all the concentrations showed significant differences in cytotoxicity except at 50 µM and 25 µM of BBR NP-**17** and 50 µM of BBR NP-**18**. The predominant difference in inhibitions may be due to the elevated levels of GSH and decreased pH conditions in the cancer cells that cleaved the disulfide and ester bonds present in the modified redox-cholesterol of the lipid matrix. Further, following erosion of the lipid matrix, the BBR is released into the cytoplasm, thereby inducing increased cytotoxicity. In contrast, BEAS-2B and HEK293A cells with low GSH levels exhibited lower cytotoxicity due to slower diffusion or release of drugs from the nanocarrier system.

Furthermore, the presence of positively charged aminated polyethylene glycol diamine in the core of the nanocarrier system may contribute to increased cytotoxicity. Upon degradation of the lipid matrix, this component may become exposed, potentially leading to binding with negatively charged membranes, thereby inducing increased BBR release and cytotoxic effects.[54]

In comparison to both the batches, BBR NP-**18** showed ~3.23 and 15.73 folds decreased IC_{50} in BEAS-2B and HEK293A cells after 24 h incubation, while only ~1.13 and 2.14 folds in the case of BBR NP-**17**. After 72 h incubation, BBR NP-**18** treated group resulted in ~3.85- and 3.27-fold reductions in IC_{50} values in BEAS-2B and HEK293A cells respectively, while only ~1.20 and 2.11 folds in the case of BBR NP-**17** (Table 4). The enhanced selectivity of BBR NP-**18** is likely due to the incorporation of stearic acid in the lipid matrix, which increases lipophilicity, slows BBR release, and prevents rapid degradation, which is in correspondence with the results observed in *in vitro* release studies (section 3.3).

Advantage of the nanoparticular form of BBR over free form of BBR

Both optimized redox-sensitive nanocarriers exhibited notably high cytotoxicity in H1975 cancer cells compared to free form of BBR after 24 and 72 h of treatment (Fig 5B, i-iv). This significant cytotoxicity observed in the group treated with BBR nanocarriers may be due to the enhanced penetration and sustained release of BBR from the nanocarriers, which was also observed in the cellular uptake studies. The difference in cytotoxicity induced by free form of BBR was observed to be non-significant in normal and cancer cells, possibly due to the non-specific release and penetration of the drug in both cells.

A biocompatibility study was performed on the blank nanocarriers (BLK NP-**17** and **18**) to assess their independent cytotoxicity. Here, different concentrations (3.125 to 50 µM with respect to BBR concentration used in cytotoxicity studies) were treated in BEAS-2B, HEK293A, and H1975 cells for 24 and 72 h incubation periods. As demonstrated in Fig. S7, greater than 75% of cells are observed to be viable in all concentrations except 50 µM concentration at both 24 and 72 h incubation periods. These findings indicate no significant toxic effects on healthy cells (<50 µM), that confirms the good biocompatibility and ensuring a safe carrier for the delivery of drugs to cancer cells. The study confirmed that the cytotoxicity induced by the nanocarriers is solely due to the selective release of up taken BBR into the cytoplasm of the cancer cell that further induced enhanced cytotoxicity.

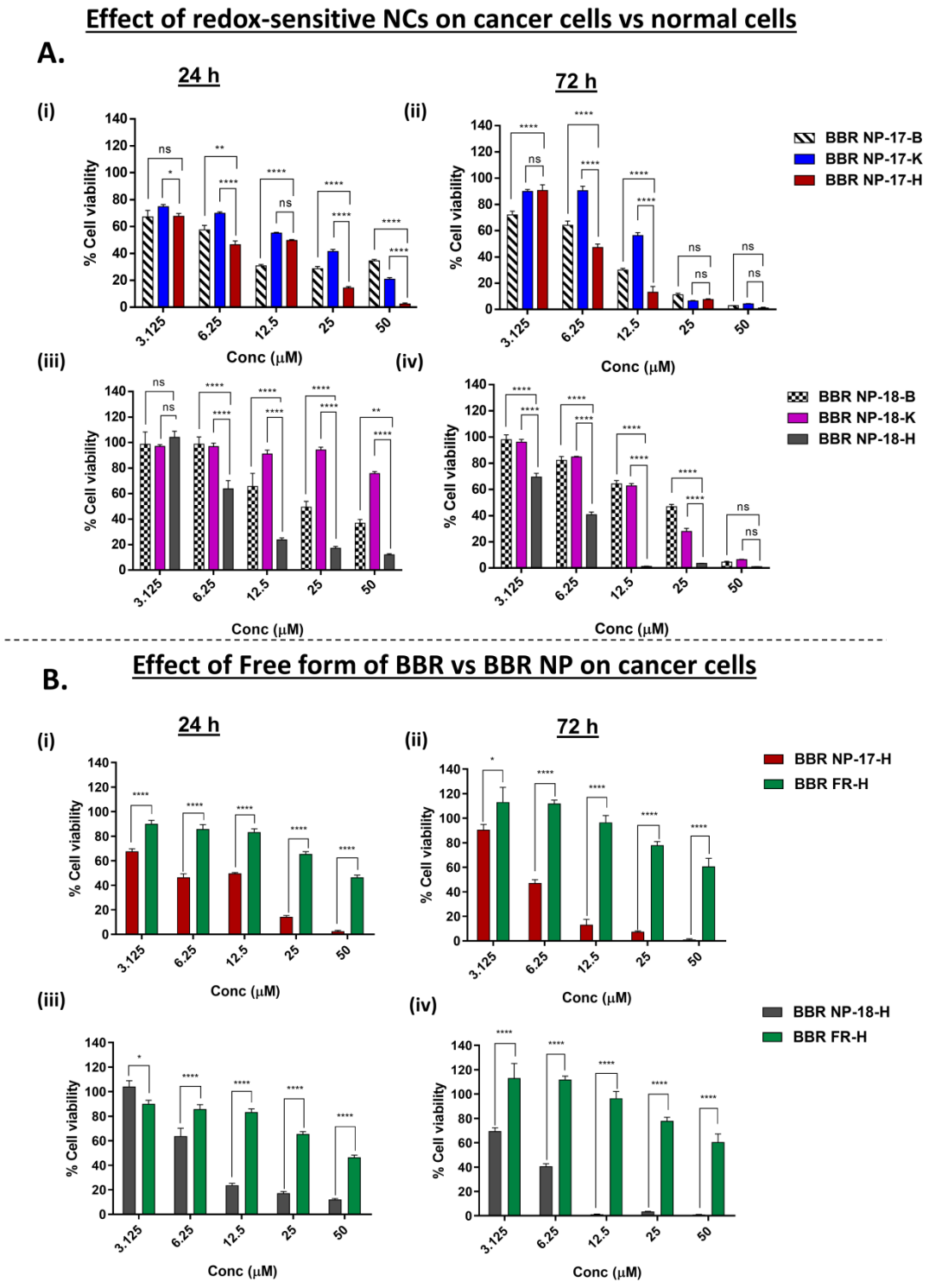

Fig. 5. Effect of redox-sensitive NCs on cancer versus normal cells. %Cell viability of BEAS-2B, HEK293A, and H1975 cells after BBR NP-**17** and **18** treatments for 24 and 72 h (A). **Effect of free form of BBR versus BBR NPs on cancer cells**. **%**Cell viability of H1975 cells after treatment with BBR in free form and nanoparticulate forms (BBR NP-**17** and **18)** for 24 and 72 h (B). All the values are expressed in mean ± SEM (n=5). A two-way ANOVA was used to compare the %cell viability difference between BEAS-2B and H1975,

as well as between HEK293A and H1975 following treatment. Additionally, a two-way ANOVA was conducted to compare the %cell viability differences in H1975 cells treated with free-form of BBR and BBR nanoparticulate forms (BBR NP-**17** and NP-**18**). Differences in p-values, *p<0.05, **p< 0.01, ***p<0.001, ****p<0.0001 were considered statistically significant and ns was considered non-significant.

Abbreviations:

H: H1975 (lung cancer cell line). **BBR NP-17-H**: H1975 cells treated with BBR NP-**17** nanocarriers, **BBR NP-18-H**: H1975 cells treated with BBR NP-**18** nanocarriers, **BBR FR-H**- refers to H1975 cells treated with free form of BBR.

B: BEAS-2B (normal lung epithelial cells). **BBR NP-17-B:** BEAS-2B cells treated with BBR NP-**17** nanocarriers, **BBR NP-18-B:** BEAS-2B cells treated with BBR NP-**18** nanocarriers.

K: **HEK293A** (normal human embryonic kidney cells). **BBR NP-17-K:** HEK293A cells treated with BBR NP-**17** nanocarriers, **BBR NP-18-K:** HEK293A cells treated with BBR NP-**18** nanocarriers

Table 4 Half maximal inhibitory (IC_{50}) concentration for BBR-loaded RS-PLHNCs and free form of BBR in BEAS-2B, HEK293A, and H1975 cells (n=5)

After 24 h incubation						
Batch no	**IC_{50} of NPs (in µM)**			**IC_{50} of free form of BBR (in µM)**		
	BEAS-2B	HEK293A	H1975	BEAS-2B	HEK293A	H1975
BBR NP-**17**	7.7 ± 1.2	14.6 ± 1.1	6.8 ± 1.1	52.8 ± 1.1	47.1 ± 1.2	46.2 ± 1.1
BBR NP-**18**	27.5 ± 1.1	133.3 ± 1.3	8.5 ± 1.1			
After 72 h incubation						
BBR NP-**17**	7.7 ± 1.2	13.1 ± 1.0	6.8 ± 1.1	40.6 ± 1.2	22.1 ± 1.1	59.6 ± 1.2
BBR NP-**18**	27.5 ± 1.1	133.3 ± 1.3	8.5 ± 1.1			

To validate the findings of BBR-induced cytotoxicity observed in the MTT assay, cellular viability was further assessed by examining cell numbers in the presence of BBR nanocarriers (IC_{50}) and free form of BBR (IC_{50} values respective to BBR NP-**17** and **18** nanocarriers were used). Notably, treatment with BBR NP-**17** and BBR NP-**18** resulted in reductions of 56.54% and 48.73% in cell numbers respectively, whereas BBR FR-**17** and BBR FR-**18** exhibited lesser reductions of 78.95% and 72.16%, respectively (Fig. S8). Taken together, data obtained from both the MTT assay and cell counting, the IC_{50} for BBR-NP **17**

and **18** was determined to be 6.79 ± 1.1 μM and 8.47 ± 1.1 μM, respectively. These findings contribute to the comprehensive understanding of the efficacy of BBR nanocarrier formulations in inducing cytotoxic effects for potential therapeutic applications.

3.5.3. Effect of BBR-loaded RS-PLHNCs on intracellular GSH Levels

Cancer cells produce high levels of antioxidants in the form of cellular free thiol, resulting in a highly reducing TME that prevents DNA damage and evades programmed cell death.[61] Moreover, GSH is overexpressed in various cancers at concentrations approximately ten times higher than normal cells (~10 mM).[62] Further, to know the effect of RS-PLNCs in GSH responsive environment we aimed to monitor GSH levels with different treatment regimens over 24 h. As illustrated in Fig. S9, our findings revealed a significant reduction in GSH levels in cells treated with BBR-loaded RS-PLHNCs formulations compared to those treated with free form of BBR. This reduction was observed across a range of concentrations, suggesting that the nanoparticulate delivery system enhances the efficacy of BBR by promoting a more pronounced depletion of GSH within cancer cells. These results provide compelling evidence that selective release of BBR from nanoparticulate formulations exert a potent pro-oxidant effect within cancer cells, disrupting their redox balance and sensitizing them to oxidative stress-induced cell death.

3.5.4. BBR-loaded RS-PLHNCs increase cellular uptake significantly

The effectiveness of drug delivery is strongly correlated to how well cells uptake the drugs. A robust cellular uptake of drugs can lead to effective treatment outcomes.[63] BBR is a fluorescent compound with excitation and emission wavelength of 345 nm and 575 nm. Therefore, the cellular uptake study was performed in normal cells (BEAS-2B and HEK293A) to evaluate the selectivity of the nanoparticulate formulations of BBR NP-**17** and BBR NP-**18** through FACS and confocal microscopy. Comparative analysis of mean fluorescence intensity (MFI) of free and nanoparticulate forms of BBR demonstrate less internalization in BEAS-2B and HEK293A at 4, 12, and 18 h in comparison to that observed in H1975 cells. Also, the free form of BBR and BBR NP-**17** & BBR-NP-**18** treated cells showed right shift of histogram peak in H1975 cells (Fig. 6A). The results from the extent of BBR cellular uptake in free and NP form directly correlates with the cytotoxicity studies where less viable cancer cells were seen in the BBR-NP-**17** & **18** treated cells compared to those treated in its free form at equal amounts.

Furthermore, CLSM was used to confirm and visualize the intracellular distribution of internalized free form of BBR and BBR-nanoparticulate form. Post treatment of BBR NP-**17** and NP-**18** for 4 and 18 h, fluorescence intensity was found to be lower in normal cells compared to cancer cells. Moreover, the fluorescence intensity of free form of BBR (BBR FR-**17** & FR-**18**) was significantly lower across all cell lines over nanoparticulate formulation of BBR (Fig. 6B), which was consistent with flow cytometry results that RS-PLHNCs remarkably enhanced BBR uptake. This observation is likely due to the limited permeability of free form of BBR, a limitation that was overcome by encapsulation within nanoparticles, thereby enhancing cellular uptake and fluorescence signal. Therefore, our findings suggest loading BBR in RS-PLHNCs follows a greater selectivity and preferential uptake in the tumor cells bypassing the cell membrane and inducing increased cytotoxicity.

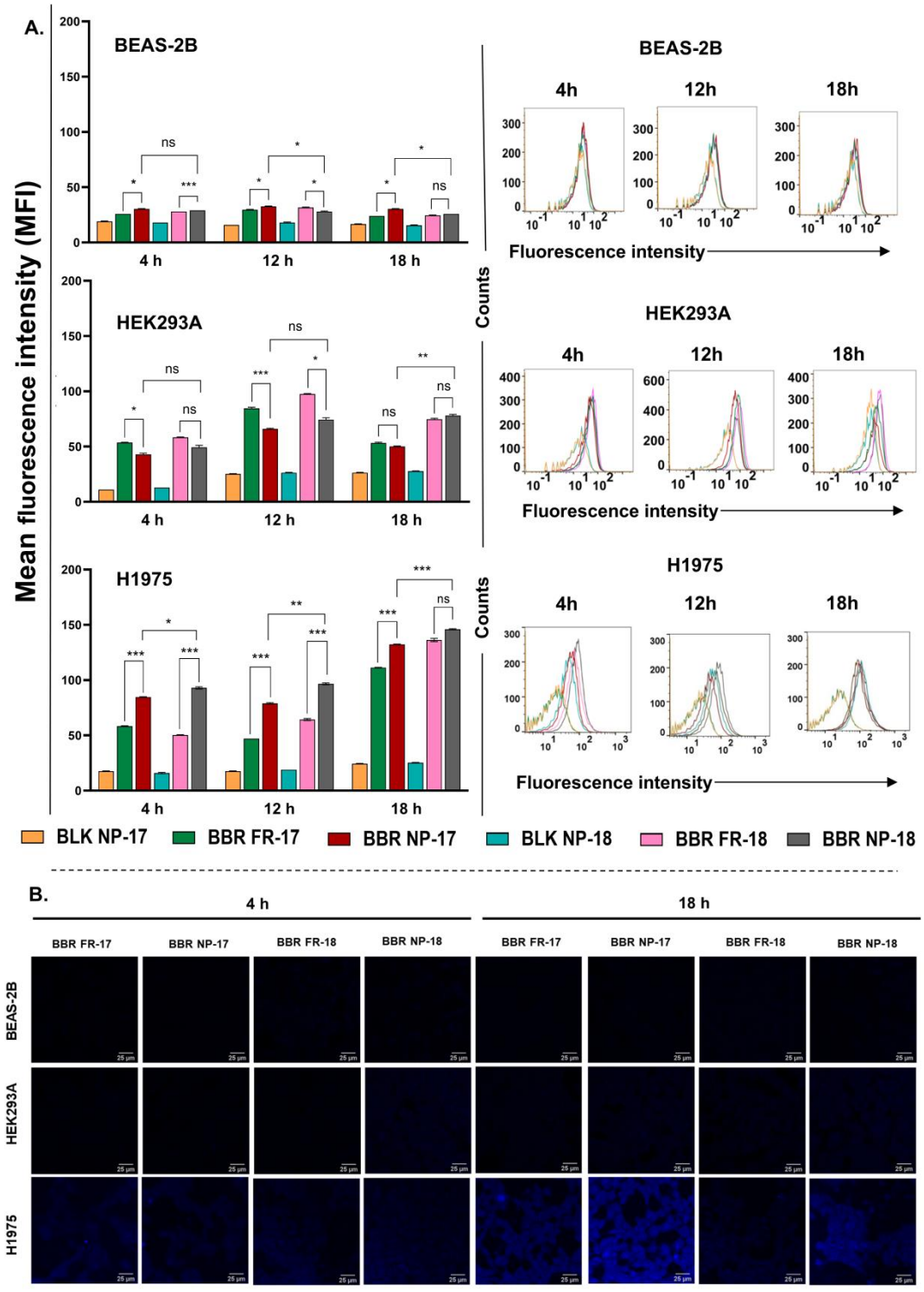

Fig. 6. Cellular uptake of BBR-loaded RS-PLHNCs and free form of BBR in BEAS-2B, HEK293A, and H1975 cells. Histograms showing the intensity of uptake for Blank NP, Free form of BBR, and BBR NP (batch **17** & **18**) at 4 h, 12 h, and 18 h and their quantitative mean fluorescence intensity (MFI) (n=3) (λ_{ex} = 488 nm; λ_{em} = 585 nm) (A). Confocal microscopy images showing intracellular fluorescence of BBR (λ_{ex} = 405 nm; λ_{em} = 550 ± 50 nm) (B). The values were statistically examined using a two-way ANOVA test. Statistical

significance: *p < 0.05, **p < 0.01, ***p < 0.001 and ns- non-significant.

Abbrerbiation: BLK NP-**17** (Blank nanoparticle in equivalent with IC_{50} of BBR NP-**17** i.e. 6.8µM); BLK NP-**18** (Blank nanopaticle in equivalent with IC_{50} of BBR NP-**18** i.e. 8.5µM); BBR FR-**17** (Free form of BBR in equivalent with IC_{50} of BBR NP-**17** i.e. 6.8µM); BBR FR-**18** (Free form of BBR in equivalent with IC_{50} of BBR NP-**18** i.e. 8.5µM); BBR NP-**17** (BBR loaded RS-PLHNCs with an IC_{50} dose of 6.8µM); BBR NP-**18** (BBR loaded RS-PLHNCs with an IC_{50} dose of 8.5µM)

783 *3.5.5. Nanoparticulate form of BBR induces apoptosis*

784 Apoptosis, a programmed cell death mechanism essential for eliminating damaged cells, is
785 often evaded in cancer, allowing tumor cells to survive and proliferate uncontrollably.[64] To
786 evaluate the effects of the nanoparticulate formulations of berberine (BBR NP-**17** and BBR
787 NP-**18**) at their respective IC_{50} values was conducted through time kinetic manner using flow
788 cytometry. Cells were stained with Annexin V-FITC/PI and analyzed at 4, 12, and 18 h post-
789 treatment in H1975, HEK293A, and BEAS-2B cell lines (Fig. 7A). At the 4 h time point,
790 BBR NP-**17** and BBR NP-**18** induced significantly higher levels of apoptotic cell death in
791 H1975 cells, compared to the normal cell lines. Specifically, 21.93 ± 1.04% and 39.17 ±
792 0.98% of H1975 cells underwent apoptosis, respectively, for BBR NP-**17** and BBR NP-**18**. In
793 contrast, BEAS-2B cells showed lower apoptosis rates (12.7 ± 0.06% and 26.83 ± 0.13%),
794 while HEK293A cells exhibited minimal apoptosis (1.47 ± 0.03% and 2.5 ± 1.10%). At 12 h,
795 the apoptotic cell death in H1975 is significantly higher, when treated with BBR NP-**17**
796 (28.80 ± 0.17%) and NP-**18** and 29.30 ± 3.40%), except comparison with HEK293A. In
797 normal cells, BBR NP-**17** significantly induces less apoptosis 4.97 ± 0.24% (BEAS-2B) and
798 12.03 ± 1.33% (HEK293A) while, treatment with NP-**18** shows 8.30 ± 0.42% and 24.23 ±
799 0.32% in BEAS-2B and HEK293A respectively. In time kinetics manner, at 18 h the
800 apoptotic cell death remained higher in H1975 cells (15.8 ± 0.64% and 11.03 ± 1.41%), while
801 BEAS-2B and HEK293A cells showed significantly lower apoptosis (4.07 ± 0.87% and 4.87
802 ± 0.19%, and 5.8 ± 0.20% and 4.37 ± 0.23%, respectively.

803 During apoptosis, the breakdown of membrane asymmetry leads to the relocation of
804 phosphatidylserine (PS) to the outer membrane layer, which can be detected by Annexin V-
805 FITC staining.[65] We further validate our finding by evaluating the apoptotic potential of RS-
806 PLHNCs loaded with BBR drug, which was visualized using CLSM. Staining with Annexin

V-FITC revealed clear signs of apoptosis when H1975 cells were incubated with BBR NP-**17** and BBR NP-**18** (Fig. 7B). Strong green fluorescence-labeled cells were observed compared to free form of BBR, where Annexin V-FITC was used as a negative control. In addition, upon BBR NP-**17** and NP-**18** treatment in BEAS-2B and HEK293A the green fluorescence intensity was lower, clearly indicating less apoptosis. These findings indicate that the BBR-loaded RS-PLHNCs follows higher cellular uptake which preferentially induce apoptotic cell death in cancer cells over normal cells, possibly due to the effective BBR release rate inside the cell, which was further validated by gene expression studies.[66]

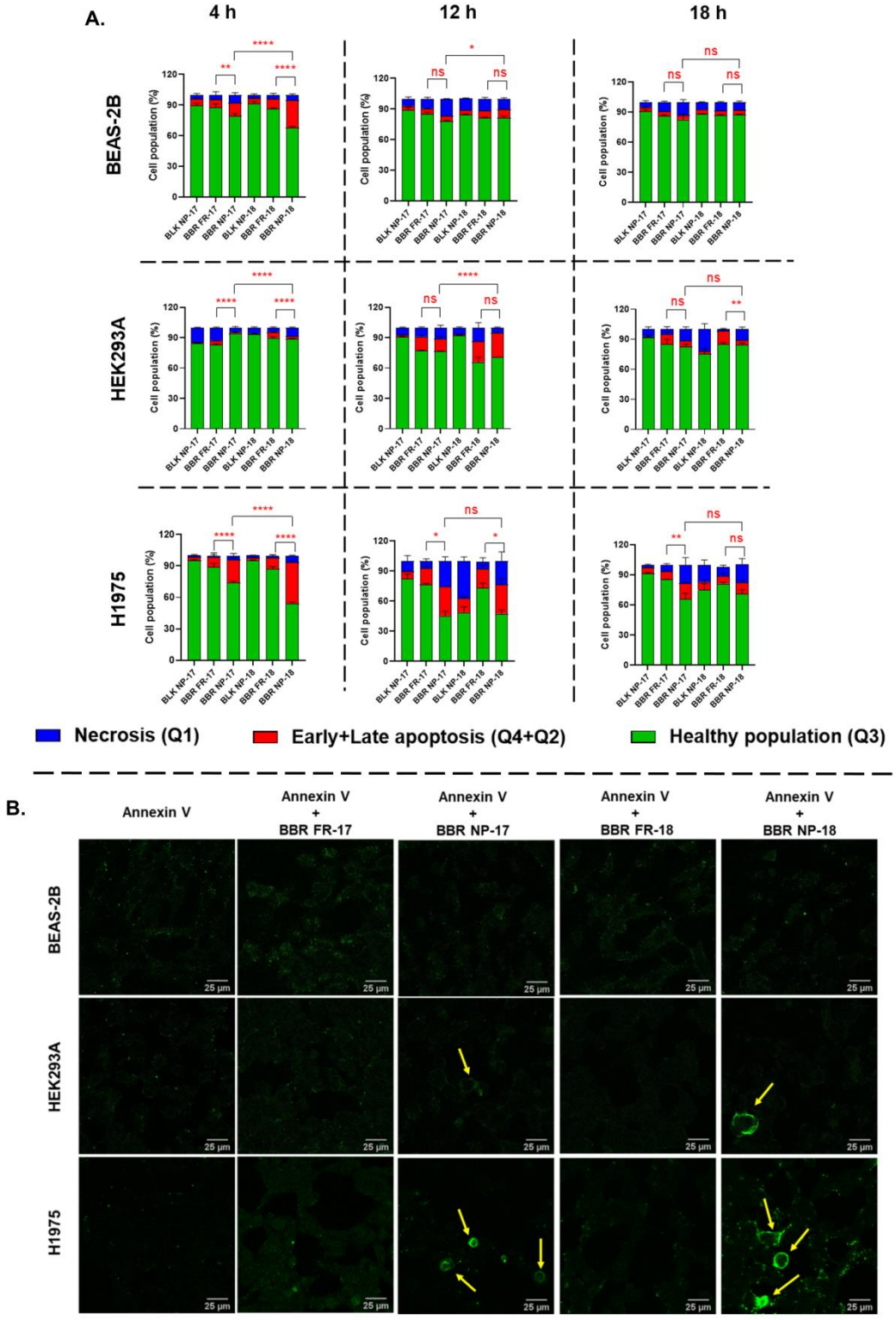

Fig. 7. Apoptosis study of free form of BBR and its nanoparticulate form (BBR NP-**17** and **18**) in BEAS-2B, HEK293A, and H1975 cells assessed via flow cytometry and confocal microscopy. Flow cytometry analysis of the % apoptotic cells determined by Annexin V-FITC/PI staining, following treatment at 4, 12, and 18 h (A).

Representative confocal images for apoptosis in Annexin V-FITC stained BEAS-2B, HEK293A, and H1975 cells after 18 h of treatment (λ_{ex} = 488 nm; λ_{em} = 550 ± 50 nm) (B). (*Yellow* arrow indicates apoptotic cells). The values were statistically examined to assess apoptotic cell death (% early+late apoptosis) by two-way ANOVA test. Statistical significance: *p < 0.05, **p < 0.01, ***p < 0.001, ****p < 0.0001, and ns- non-significant.

3.5.6. BBR-loaded RS-PLHNCs induce oxidative stress and cause apoptosis

The oxidative stress in cancer cells ameliorates redox balance, thus increasing antioxidant states and optimizing ROS-driven proliferation.[67] In this context, superoxide dismutase (SOD), catalase, glutathione peroxidase (GPX), and thioredoxin (TRX) are the key regulators in counteracting by maintaining the reduced state of NADPH. Aberrant oxidative stress acts upon several biochemical pathways and signaling proteins such as MAPK, PI3K/AKT, and KEAP1-NRF2 pathways.[68] Among these Nrf2, a master transcription factor provides a principle inducible defense against oxidative stress and activates a wide range of target genes SOD1, xCT, HO-1, NQO1, TXRND1, and GCLC.[69,70] Here, we investigated the effect of nanoparticulate BBR and free form of BBR on mRNA expression levels of NFE2L2, HO-1, NQO1, and TXRND1 performed by qRT-PCR.

The relative mRNA expression of NFE2L2 was significantly downregulated by **~0.1 fold** and **~0.3-fold** change in BBR NP-**17** & BBR NP-**18**. In contrast, **~0.9 fold** and **~0.7-fold** change was observed in BBR FR-**17** & BBR FR-**18** when compared to the control group (Fig. 8A). NAD(P)H: quinone oxidoreductase-1 is a phase detoxifying enzyme, and overexpressed in ~60% of NSCLC cases.[71,72] NQO1 and HMOX1 mRNA expression was found to be significantly downregulated by **~0.3 fold** and **~0.4 fold**, & **~0.6 fold** and **~0.5 fold** change in nanoparticulate form of BBR-**17** & BBR-**18**, when compared to control group, respectively. Upon BBR FR-**17** & BBR FR-**18** treatment, the NQO1 and HMOX1 mRNA expression was unaltered (Fig. 8B & 8C). TXRND1 amid among NRF2 target redox genes signature in NRF2/KEAP1 axis, with poor survival in a cohort of NSCLC patients.[73] A significantly downregulated mRNA expression of TXRND1 gene with **~0.3 fold** and **~0.3 fold** change in BBR NP-**17** & BBR NP-**18**, and **~1.1 fold** and **~0.8 fold** change in BBR FR-**17** and BBR FR-**18** when compared to the control group (Fig. 8D). In addition, for genes mentioned above, BBR NP-**17** & BBR NP-**18** found to be significantly upregulated when compared to free form of BBR.

Berberine inhibits cell proliferation and induces apoptosis in breast, lung, and liver cancer via the BCL-2/BAX pathway.[74,75] Based on previous studies, we aimed to evaluate the effect of BBR nanoparticulate on apoptotic markers such as PUMA, NOXA, and MCL-1. The mRNA expression of PUMA and NOXA was significantly upregulated upon BBR NP-**17** and BBR NP-**18** by **~7.3 fold** and **~4.4-fold** change, whereas **~3.2 fold** and **~2.0-fold** difference was observed in BBR FR-**17** & BBR FR-**18** group when compared with control group respectively (Fig. 8E & F). MCL-1 is a key anti-apoptotic marker of the BCL-2 family, often overexpressed in tumors, promoting cell survival and drug resistance. Targeting MCL-1 holds promise for cancer therapy due to its central role in blocking apoptosis via the mitochondrial pathway.[76,77] Upon BBR NP-**17** & BBR NP-**18** treatment, significant downregulation by **~0.1-fold** and **~0.2-fold** was observed compared to the control group treatment (Fig. 8G). Additionally, BBR NP-**17** & BBR NP-**18** showed significant upregulation of PUMA and NOXA and down-regulation of MCL-1, respectively, compared to BBR FR-**17** & BBR FR-**18**. The results suggest that BBR NP-**17** has better therapeutic efficacy than BBR NP-**18** by increasing the oxidative stress and inducing apoptosis.

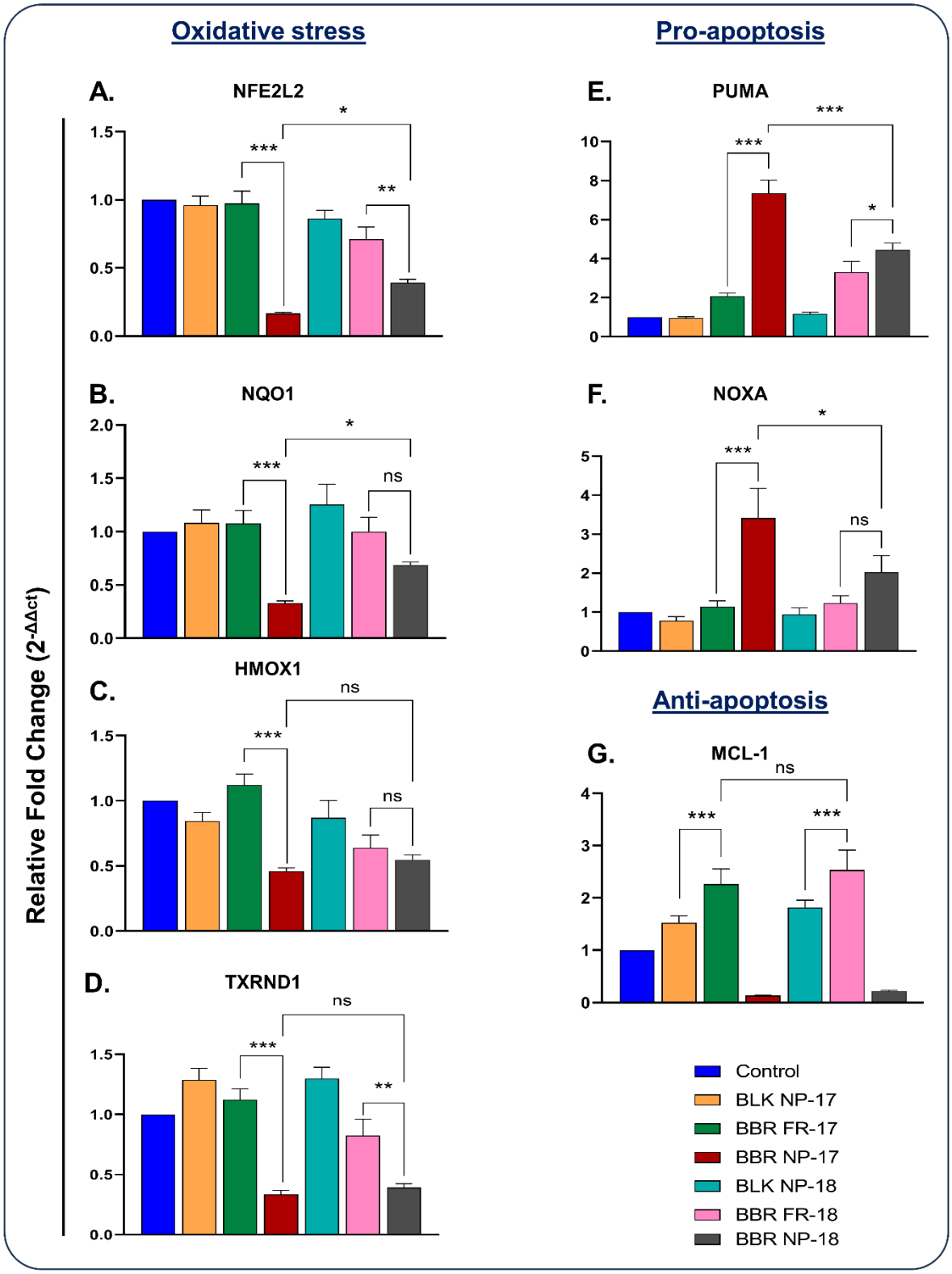

Fig. 8. The Nanoparticulate form of BBR promotes apoptosis and lowers oxidative stress in NSCLC (H1975 cells). The relative mRNA expression of (A-D). **Oxidative stress markers** (A). NFE2l2 (B). NQO1, (C). HMOX1, and (D). TXRND1. (E-G). **Pro-apoptotic markers** PUMA (E). and NOXA (F). **Anti-apoptotic markers** (G). MCL-1. The data are represented

as mean ± SEM (n = 4), and statistical significance was performed using a one-way ANOVA test. Statistical significance was denoted as follows: *p < 0.05, **p < 0.01, ***p < 0.001 and "ns" indicating non-significant differences.

4. Conclusion

In the current study, bioreducible **r**edox-**s**ensitive **p**olymeric **l**ipid **h**ybrid **n**anocarriers (RS-PLHNCs) were successfully fabricated and characterized. The optimized monodispersible BBR-loaded nanocarriers (BBR NP-**17** and **18**) demonstrated acceptable particle sizes (124 and 185 nm) with good encapsulation efficiency (>80%). These novel nanocarriers displayed accelerated BBR release (>80% in 24 h) on exposure to tumor-relevant pH (pH 4.5-5.5) and reduction environment (10mM GSH) relative to physiological conditions (30-45% in 24 h). This increased release is due to the reduction of disulfide bonds in the GSH reductive environment (disulfide bonds present in modified cholesterol of lipid matrix layer surrounding the polymer core) and hydrolysis of ester bonds in acidic pH, leading to the disassembly of nanocarriers, thereby increasing the release of BBR. These dual-stimuli-triggered nanocarriers exhibited selective cytotoxicity against H1975 (NSCLC) cells over normal BEAS-2B and HEK293A cells. Moreover, these nanocarriers displayed several-fold increased cytotoxicity than free form of BBR. This enhanced killing efficiency might be due to the increased penetration of nanocarriers by the EPR effect compared to the free form of the drug, as observed in the cellular uptake studies. The several underlying mechanisms for the enhanced anti-cancer activity are due to the downregulation of NFE2L2, HO-1, NQO1, and TXRND1 gene expression, and decreased GSH levels leading to oxidative stress, thereby causing apoptosis of the cancer cells. In summary, the selective uptake and cytotoxicity of the designed novel redox-responsive nanocarriers in cancer cells have promising implications for targeted drug delivery in lung cancer treatment, thereby reducing drug-related toxicities. To our knowledge, till date no study has reported the design and synthesis of a redox-responsive nanocarrier loaded with BBR, specifically engineered for targeted delivery to cancer cells.

In summary, our study presents bioreducible redox-sensitive polymeric lipid hybrid nanocarriers (RS-PLHNCs) synthesized for targeted delivery of BBR in NSCLC cells. The optimized BBR-loaded nanocarriers (NP-17 & -18) exhibited effective particle size with higher encapsulation efficiency and sustained the release of BBR in tumor simulated microenvironment (acidic pH and 10mM GSH). These nanocarriers showed preferential

uptake in NSCLC cells compared to normal cells due to their increased permeability and retention (EPR) effect. Moreover, they displayed cancer cell selective cytotoxicity by increasing oxidative stress, causing apoptosis, and demonstrating significant anticancer activity. This study found novel applications for BBR-loaded RS-PHLNCs, opening new avenues toward reducing toxicity and increasing therapeutic outcomes from redox-sensitive stimuli.

In summary, developing biocompatible BBR-loaded bioreducible **r**edox-**s**ensitive **p**olymeric **l**ipid **h**ybrid **n**anocarriers (RS-PLHNCs) demonstrates a promising strategy for the selective delivery of BBR to GSH-rich cancer cells. The optimized BBR nanocarriers (NP-**17** & -**18**) exhibited optimal particle size with higher encapsulation efficiency and sustained the release of BBR in tumor simulated microenvironment (acidic pH and 10mM GSH). The redox-sensitive nature of these nanocarriers displayed preferential uptake of BBR in NSCLC cells compared to normal cells due to their increased GSH levels and EPR effect. Moreover, they displayed cancer cell-selective cytotoxicity by increasing oxidative stress, causing apoptosis, and demonstrating significant anticancer activity. Thus, prepared redox-responsive nanocomposite material can be further used to precisely deliver similar bioactive compounds by enhancing their pharmaceutical properties and preventing non-selective toxic effects, thereby improving treatment outcomes in cancer therapy.

Conflict of interests

The authors declare that they have no conflict of interest.

Funding

This work was fully supported by intramural funding (DPR) from the National Institute of Science Education and Research (NISER), the Department of Atomic Energy (DAE), Government of India (GoI).

Acknowledgments

The authors thank the full financial support by intramural funding (DPR) received from National Institute of Science Education and Research (NISER), Department of Atomic Energy (DAE), Government of India (GoI). B.S.L., R.C., and S.K.M., would like to acknowledge NISER, DAE, GoI for the research fellowship. The authors would also like to acknowledge the support provided by TEM imaging facility, Centre for Interdisciplinary

Sciences (CIS), NISER, for their assistance in TEM imaging and Dr. Tathagata Mukherjee, Somlata Khamaru, and Kshyama Subhadarsini Tung, School of Biological Sciences (SBS), NISER, during FACS analysis. The authors also acknowledge Dr. Amit Jaiswal, IIT-Mandi, India, for helping with the HEK293A cell line for *in vitro* cell based studies. The authors are thankful to acknowledge Dr. Soumendra Rana, IIT-Bhubaneswar, India, for mass characterization.

Authors Affiliations

School of Biological Sciences, National Institute of Science Education and Research, HBNI, Jatni, Odisha 752050, India

B. Siva Lokesh, Suresh Ajmeera, Rajat Choudhary, V Badireenath Konkimalla

School of Chemical Sciences, National Institute of Science Education and Research, HBNI, Jatni, Odisha 752050, India

Sanjaya Kumar Moharana and C. S. Purohit

Homi Bhabha National Institute, Training School Complex, Anushaktinagar, Mumbai 400094, India

B. Siva Lokesh, Rajat Choudhary, Sanjaya Kumar Moharana, C. S. Purohit, V. Badireenath Konkimalla

Hasselt University, Institute for Materials Research (IMO), Nano-Biophysics and Soft Matter Interfaces (NSI), Wetenschapspark 1, 3590 Diepenbeek, Belgium

Suresh Ajmeera

IMEC, associated lab IMOMEC, Wetenschapspark 1, 3590 Diepenbeek, Belgium

Suresh Ajmeera

Corresponding author

Correspondence to Dr. V Badireenath Konkimalla (badireenath@niser.ac.in)

Author contributions

B. Siva Lokesh: Conceptualization, Methodology, Investigation, Data curation, Formal analysis, Writing - original draft, preparation. **Suresh Ajmeera:** Conceptualization, Methodology, Investigation, Data curation, Formal analysis, Writing - original draft, preparation. **Rajat Choudhary:** Conceptualization, Methodology, Investigation, Data curation, Formal analysis, Writing - original draft, preparation. **Sanjaya Kumar Moharana:** Characterization and analysis of synthesized lipids and polymers. **C. S. Purohit:** Formal analysis and supervision of synthesized lipids and polymers. **V. Badireenath Konkimalla:** Conceptualization, Formal analysis, Supervision, Resources, Funding acquisition, Project administration, Writing – original draft, Writing – review & editing.

References

1 F. Raza, H. Zafar, X. You, A. Khan, J. Wu and L. Ge, *J. Mater. Chem. B*, 2019, **7**, 7639–7655.

2 L. Sun, H. Liu, Y. Ye, Y. Lei, R. Islam, S. Tan, R. Tong, Y.-B. Miao and L. Cai, *Signal Transduct. Target. Ther.*, 2023, **8**, 418.

3 S. Krishnamurthy, R. Vaiyapuri, L. Zhang and J. M. Chan, *Biomater. Sci.*, 2015, **3**, 923–936.

4 C. Corbet and O. Feron, *Nat. Rev. Cancer*, 2017, **17**, 577–593.

5 D. C. Singleton, A. Macann and W. R. Wilson, *Nat. Rev. Clin. Oncol.*, 2021, **18**, 751–772.

6 S. Son, N. V. Rao, H. Ko, S. Shin, J. Jeon, H. S. Han, V. Q. Nguyen, T. Thambi, Y. D. Suh and J. H. Park, *Int. J. Biol. Macromol.*, 2018, **110**, 399–405.

7 Y. Chi, X. Yin, K. Sun, S. Feng, J. Liu, D. Chen, C. Guo and Z. Wu, *J. Control. Release*, 2017, **261**, 113–125.

8 R. Yan, X. Liu, J. Xiong, Q. Feng, J. Xu, H. Wang and K. Xiao, *RSC Adv.*, 2020, **10**, 13889–13899.

9 X. Peng, P. Liu, B. Pang, Y. Yao, J. Wang and K. Zhang, *Carbohydr. Polym.*, 2019, **216**, 113–118.

10 D. D. Gurav, A. S. Kulkarni, A. Khan and V. S. Shinde, *Colloids Surf. B. Biointerfaces*, 2016, **143**, 352–358.

11 J. Yu, H. Deng, F. Xie, W. Chen, B. Zhu and Q. Xu, *Biomaterials*, 2014, **35**, 3132–44.

12 M. G. Adimoolam, N. Amreddy, M. R. Nalam and M. V. Sunkara, *J. Magn. Magn. Mater.*, 2018, **448**, 199–207.

13 Q. Chen, H. Ding, J. Zhou, X. Zhao, J. Zhang, C. Yang, K. Li, M. Qiao, H. Hu, P. Ding and X. Zhao, *RSC Adv.*, 2016, **6**, 17782–17791.

14 Y. Li, A. Lu, M. Long, L. Cui, Z. Chen and L. Zhu, *Acta Biomater.*, 2019, **83**, 334–348.

15 J. Wang, G. Su, X. Yin, J. Luo, R. Gu, S. Wang, J. Feng and B. Chen, *Biomed. Pharmacother.*, 2019, **120**, 1–8.

16 B. Lu, F. Xiao, Z. Wang, B. Wang, Z. Pan, W. Zhao, Z. Zhu and J. Zhang, *ACS Biomater. Sci. Eng.*, 2020, **6**, 4106–4115.

17 C. Hald Albertsen, J. A. Kulkarni, D. Witzigmann, M. Lind, K. Petersson and J. B. Simonsen, *Adv. Drug Deliv. Rev.*, 2022, **188**, 114416.

18 Z. Li, W. Qiao, C. Wang, H. Wang, M. Ma, X. Han and J. Tang, *Drug Deliv.*, 2020, **27**, 736–744.

19 T. J. Chirayil and G. S. Vinod Kumar, *Int. J. Nanomedicine*, 2022, **17**, 5099–5116.

20 B. Siva Lokesh, P. Haloi and V. B. Konkimalla, *J. Drug Deliv. Sci. Technol.*, 2023, **80**, 104101.

21 K. Thananukul, C. Kaewsaneha, P. Opaprakasit, N. Zine and A. Elaissari, *Sci. Rep.*, 2022, **12**, 1–14.

22 F. A. Younis, S. R. Saleh, S. S. A. El-Rahman, A.-S. A. Newairy, M. A. El-Demellawy and D. A. Ghareeb, *Sci. Rep.*, 2022, **12**, 17431.

23 A. Agnarelli, M. Natali, M. Garcia-Gil, R. Pesi, M. G. Tozzi, C. Ippolito, N. Bernardini, R. Vignali, R. Batistoni, A. M. Bianucci and S. Marracci, *Sci. Rep.*, 2018, **8**, 10599.

24 Y. S. Loo, T. Madheswaran, R. Rajendran and R. J. Bose, *J. Drug Deliv. Sci. Technol.*, 2020, **57**, 101756.

25 K. Zou, Z. Li, Y. Zhang, H. Y. Zhang, B. Li, W. L. Zhu, J. Y. Shi, Q. Jia and Y. M. Li, *Acta Pharmacol. Sin.*, 2017, **38**, 157–167.

26 M. Farahani, F. Moradikhah, I. Shabani, R. K. Soflou and E. Seyedjafari, *J. Drug Deliv. Sci. Technol.*, 2021, **61**, 102134.

27 X. Ma, E. Özliseli, Y. Zhang, G. Pan, D. Wang and H. Zhang, *Biomater. Sci.*, 2019, **7**, 634–644.

28 P. Xue, D. Liu, J. Wang, N. Zhang, J. Zhou, L. Li, W. Guo, M. Sun, X. Han and Y.

Wang, *Bioconjug. Chem.*, 2016, **27**, 1360–72.

29 R. Otter, N. A. Henke, C. Berac, T. Bauer, M. Barz, S. Seiffert and P. Besenius, *Macromol. Rapid Commun.*, 2018, **39**, e1800459.

30 N. Tahir, A. Madni, A. Correia, M. Rehman, V. Balasubramanian, M. M. Khan and H. A. Santos, *Int. J. Nanomedicine*, 2019, **14**, 4961–4974.

31 X. Zhao, H. Guo, H. Bera, H. Jiang, Y. Chen, X. Guo, X. Tian, D. Cun and M. Yang, *ACS Appl. Mater. Interfaces*, 2023, **15**, 4441–4457.

32 R. Ghaffari, N. Eslahi, E. Tamjid and A. Simchi, *ACS Appl. Mater. Interfaces*, 2018, **10**, 19336–19346.

33 N. S. Thakur, N. Mandal, G. Patel, S. Kirar, Y. N. Reddy, V. Kushwah, S. Jain, Y. N. Kalia, J. Bhaumik and U. C. Banerjee, *Nanomedicine*, 2021, **33**, 102368.

34 P. Haloi, B. S. Lokesh, S. Chawla and V. B. Konkimalla, *Drug Deliv.*, 2023, **30**, 2184307.

35 Y. Chen, M. Su, Y. Li, J. Gao, C. Zhang, Z. Cao, J. Zhou, J. Liu and Z. Jiang, *ACS Appl. Mater. Interfaces*, 2017, **9**, 30519–30535.

36 R. B. K C, B. Thapa and P. Xu, *Mol. Pharm.*, 2012, **9**, 2719–29.

37 L. Chen, X. Zhou, W. Nie, Q. Zhang, W. Wang, Y. Zhang and C. He, *ACS Appl. Mater. Interfaces*, 2016, **8**, 33829–33841.

38 P. Yang, L. Zhang, T. Wang, Q. Liu, J. Wang, Y. Wang, Z. Tu and F. Lin, *Onco. Targets. Ther.*, 2020, **13**, 8055–8067.

39 I. Rahman, A. Kode and S. K. Biswas, *Nat. Protoc.*, 2006, **1**, 3159–65.

40 P. Haloi, R. Choudhary, B. S. Lokesh and V. B. Konkimalla, *Immunol. Lett.*, 2024, **267**, 106854.

41 V. M. Lu, F. Crawshay-Williams, B. White, A. Elliot, M. A. Hill and H. E. Townley, *Artif. Cells, Nanomedicine Biotechnol.*, 2019, **47**, 132–143.

42 H. Li, Y. Cui, J. Liu, S. Bian, J. Liang, Y. Fan and X. Zhang, *J. Mater. Chem. B*, 2014, **2**, 3500–3510.

43 N. Tahir, A. Madni, V. Balasubramanian, M. Rehman, A. Correia, P. M. Kashif, E. Mäkilä, J. Salonen and H. A. Santos, *Int. J. Pharm.*, 2017, **533**, 156–168.

44 X. Yang, D. Salado-Leza, E. Porcel, C. R. González-Vargas, F. Savina, D. Dragoe, H. Remita and S. Lacombe, *Int. J. Mol. Sci.*, 2020, **21**, 1–20.

45 M. Das, D. Bandyopadhyay, R. P. Singh, H. Harde, S. Kumar and S. Jain, *J. Mater. Chem.*, 2012, **22**, 24652.

46 E. Jaradat, E. Weaver, A. Meziane and D. A. Lamprou, *Mol. Pharm.*, 2023, **20**, 6184–6196.

47 R. S. Fernandes, R. G. Arribada, J. O. Silva, A. Silva-Cunha, D. M. Townsend, L. A. M. Ferreira and A. L. B. Barros, *Pharmaceutics*, 2022, **14**, 2394.

48 N. Vikas, A. K. Mehata, M. K. Viswanadh, A. K. Malik, A. Setia, P. Kumari, S. K. Mahto and M. S. Muthu, *Biomacromolecules*, 2023, **24**, 4989–5003.

49 S. Comincini, F. Manai, M. Sorrenti, S. Perteghella, C. D'Amato, D. Miele, L. Catenacci and M. C. Bonferoni, *Pharmaceutics*, 2023, **15**, 1078.

50 R. Bhanumathi, K. Vimala, K. Shanthi, R. Thangaraj and S. Kannan, *New J. Chem.*, 2017, **41**, 14466–14477.

51 Y. Ding, Y. Dai, M. Wu and L. Li, *Chem. Eng. J.*, 2021, **426**, 128880.

52 B. Niu, K. Liao, Y. Zhou, T. Wen, G. Quan, X. Pan and C. Wu, *Biomaterials*, 2021, **277**, 121110.

53 X. Pang, Y. Jiang, Q. Xiao, A. W. Leung, H. Hua and C. Xu, *J. Control. Release*, 2016, **222**, 116–129.

54 W. Zhou, H. Yu, L. J. Zhang, B. Wu, C. X. Wang, Q. Wang, K. Deng, R. X. Zhuo and S. W. Huang, *Nanoscale*, 2017, **9**, 17044–17053.

55 Y. Sun, X. Du, J. He, J. Hu, M. Zhang and P. Ni, *J. Mater. Chem. B*, 2017, **5**, 3771–3782.

56 L. Sun, X. Zhang, J. An, C. Su, Q. Guo and C. Li, *RSC Adv.*, 2014, **4**, 20208–20215.

57 L. Hu, P. Zhang, X. Wang, X. Cheng, J. Qin and R. Tang, *Carbohydr. Polym.*, 2017,

178, 166–179.

58 H. Lee, K. Lee and G. P. Tae, *Bioconjug. Chem.*, 2008, **19**, 1319–1325.

59 K. R. Gajbhiye, R. Salve, M. Narwade, A. Sheikh, P. Kesharwani and V. Gajbhiye, *Mol. Cancer*, 2023, **22**, 1–44.

60 H. Thai, C. Thuy Nguyen, L. Thi Thach, M. Thi Tran, H. Duc Mai, T. Thi Thu Nguyen, G. Duc Le, M. Van Can, L. Dai Tran, G. Long Bach, K. Ramadass, C. I. Sathish and Q. Van Le, *Sci. Rep.*, 2020, **10**, 1–15.

61 C. A. Labarrere and G. S. Kassab, *Front. Nutr.*, 2022, **9**, 1–25.

62 H. J. Forman, H. Zhang and A. Rinna, *Mol. Aspects Med.*, 2009, **30**, 1–12.

63 S. Behzadi, V. Serpooshan, W. Tao, M. A. Hamaly, M. Y. Alkawareek, E. C. Dreaden, D. Brown, A. M. Alkilany, O. C. Farokhzad and M. Mahmoudi, *Chem. Soc. Rev.*, 2017, **46**, 4218–4244.

64 T. E. Ali, M. A. Assiri, M. N. Alqahtani, A. A. Shati, M. Y. Alfaifi and S. E. I. Elbehairi, *RSC Adv.*, 2023, **13**, 18658–18675.

65 R. C. Taylor, S. P. Cullen and S. J. Martin, *Nat. Rev. Mol. Cell Biol.*, 2008, **9**, 231–241.

66 D. Y. Zhang, Y. Zheng, H. Zhang, J. H. Sun, C. P. Tan, L. He, W. Zhang, L. N. Ji and Z. W. Mao, *Adv. Sci.*,2018, **5**, 1800581.

67 J. D. Hayes, A. T. Dinkova-Kostova and K. D. Tew, *Cancer Cell*, 2020, **38**, 167–197.

68 M. J. Iqbal, A. Kabeer, Z. Abbas, H. A. Siddiqui, D. Calina, J. Sharifi-Rad and W. C. Cho, *Cell Commun. Signal.*, 2024, **22**, 1–16.

69 M. Rojo de la Vega, E. Chapman and D. D. Zhang, *Cancer Cell*, 2018, **34**, 21–43.

70 A. A. Zimta, D. Cenariu, A. Irimie, L. Magdo, S. M. Nabavi, A. G. Atanasov and I. Berindan-Neagoe, *Cancers (Basel).*, 2019, **11**, 1–26.

71 B. Madajewski, M. A. Boatman, I. Martinez, J. H. Carter and E. A. Bey, *Genes (Basel).*, 2023, **14**, 607.

72 J. Wu, S. Li, C. Li, L. Cui, J. Ma and Y. Hui, *Redox Biol.*, 2021, **47**, 102170.

73 M. Delgobo, R. M. Gonçalves, M. A. Delazeri, M. Falchetti, A. Zandoná, R. Nascimento das Neves, K. Almeida, A. C. Fagundes, D. P. Gelain, J. I. Fracasso, G. B. de Macêdo, L. Priori, N. Bassani, A. J. R. Bishop, C. M. Forcelini, J. C. F. Moreira and A. Zanotto-Filho, *Free Radic. Biol. Med.*, 2021, **177**, 58–71.

74 Q. Chen, Y. Hou, D. Li, Z. Ding, X. Xu, B. Hao, Q. Xia, M. Li and L. Fan, *Ann. Transl. Med.*, 2022, **10**, 485–485.

75 Y. Zhu, N. Xie, Y. Chai, Y. Nie, K. Liu, Y. Liu, Y. Yang, J. Su and C. Zhang, *Front. Pharmacol.*, 2022, **13**, 1–19.

76 H. Wang, M. Guo, H. Wei and Y. Chen, *J. Hematol. Oncol.*, 2021, **14**, 1–18.

77 E. Munkhbaatar, M. Dietzen, D. Agrawal, M. Anton, M. Jesinghaus, M. Boxberg, N. Pfarr, P. Bidola, S. Uhrig, U. Höckendorf, A.-L. Meinhardt, A. Wahida, I. Heid, R. Braren, R. Mishra, A. Warth, T. Muley, P. S. P. Poh, X. Wang, S. Fröhling, K. Steiger, J. Slotta-Huspenina, M. van Griensven, F. Pfeiffer, S. Lange, R. Rad, M. Spella, G. T. Stathopoulos, J. Ruland, F. Bassermann, W. Weichert, A. Strasser, C. Branca, M. Heikenwalder, C. Swanton, N. McGranahan and P. J. Jost, *Nat. Commun.*, 2020, **11**, 4527.